Environmental stiffness regulates neuronal maturation via Piezo1-mediated TTR activity

Eva Kreysing[1, 2, 3,*], Hélène Gautier[1], Robert Humphrey[1,4], Katrin Mooslehner[1, 2, 3], Leila Muresan[1,5], Daniel Haarhoff[6], Sudipta Mukherjee[1], Xiaohui Zhao[7], Alexander Winkel[1], Andrea Dimitracopoulos[1], Eva K. Pillai[1], Ragnhildur Thóra Káradóttir[4,*], and Kristian Franze[1, 2, 3,*]

[1] Department of Physiology, Development and Neuroscience, University of Cambridge, Downing Street, Cambridge CB2 3DY, UK

[2] Institute of Medical Physics and Microtissue Engineering, Friedrich-Alexander-Universität Erlangen-Nürnberg, Henkestraße 91, 91052 Erlangen, Germany

[3] Max-Planck-Zentrum für Physik und Medizin, Kussmaulallee 2, 91054 Erlangen, Germany

[4] Cambridge Stem Cell Institute, Jeffrey Cheah Biomedical Centre, University of Cambridge Biomedical Campus, Puddicombe Way, Cambridge CB2 0AW, UK

[5] School of Computing and Information Science, Faculty of Science and Engineering, Anglia Ruskin University, CB1 1PT Cambridge, UK

[6] Makespace Cambridge Ltd, 16 Mill Lane, Cambridge, CB2 1RX, UK

[7] Department of Medicine, Cardiovascular Division, University of Cambridge, Heart and Lung Research Institute, CB2 0BB, Cambridge, UK

* Correspondence: Eva Kreysing (emk42@cam.ac.uk), Ragnhildur Thóra Káradóttir (rk385@cam.ac.uk), Kristian Franze (kf284@cam.ac.uk)

Abstract

During brain development, neurons extend axons to connect to their target cells while initiating a maturation process, during which neurons start expressing voltage-gated ion channels, form synapses, express synaptic transmitters and receptors, and start communicating via action potentials. Little is known about external factors regulating this process. Here, we identified environmental mechanics as an important regulator of neuronal maturation, and a molecular pathway linking tissue stiffness to this process. Using patch clamp electrophysiology, calcium imaging and immunofluorescence, we found that neurons cultured on stiffer substrates showed a delay in voltage-gated ion channel activity, spontaneous and evoked action potentials, and synapse formation. RNA sequencing and CRISPR/Cas9 knockdown strategies revealed that the mechanosensitive ion channel Piezo1 supresses transthyretin (TTR) expression on stiffer substrates, slowing down synaptic receptor expression and consequently electrical maturation. Stiffening of brain tissue in *Xenopus laevis* embryos also resulted in a significant delay of synaptic activity *in vivo*. Our data indicate that environmental stiffness represents a fundamental regulator of neuronal maturation, which is important for the development of normal circuitry in the brain, and potentially for neurodevelopmental disorders.

Introduction

Cell maturation is a fundamental aspect of the development of multicellular organisms, underlying cellular specialisation in many different cell types. During this process, cells become fully differentiated, attaining specialised features and functions. Hallmarks of cell maturation include a spectrum of changes in proliferation dynamics, gene expression profiles, metabolic activity, morphology, cellular connectivity and functionality[1].

In the nervous system, the maturation of postmitotic neurons is essential for neurons to sense, process, transmit and store information. During the maturation process, neurons extend axons and dendrites, become electrically active, form synapses, specify transmitters and transmitter receptors, and eventually form complex networks[2]. These processes are regulated mostly by genetic and epigenetic factors[3].

Some of these processes are also regulated by external factors though[3]. For example, axon outgrowth and neurotransmitters expression[4] are promoted by brain-derived neurotrophic factor (BDNF), the development of presynaptic specialisation sites in axons is regulated by netrins[5], and synapse formation is promoted by Eph/ephrin signalling through N-methyl-D-aspartate receptor (NMDAR) clustering[6]. However, the electrical maturation of neurons has been thought to be mainly cell-intrinsically regulated.

During electrical maturation, neurotransmitters, neurotransmitter receptors, and voltage-gated ion channels are expressed, enabling neuronal communicating via action potentials[7]. Electrical maturation rates are activity-dependent. For example, calcium influxes through voltage-gated ion channels regulate the differentiation of potassium current kinetics at early developmental stages[8]. Furthermore, in the human cortex the timing of neuronal maturation is regulated by epigenetic factors such as histone methylation, and the rate at which human neurons mature was recently suggested to be determined well before neurogenesis[9]. Yet, the electrical

excitability of neurons does not start simultaneously throughout the brain[10], suggesting that external signals may also exist which regulate the timing of the electrical maturation of neurons. Understanding how environmental cues regulate neuronal maturation remains a major challenge in the field[11].

In other tissues, such as cardiac tissue, mechanical stimulation enhances cell maturation[12]. Also in the CNS, tissue mechanics has been shown to instruct various neurodevelopment processes[13] including axon growth and guidance[14,15], dendrite branching[16,17] and the activity of established neuronal networks[18]. However, the precise regulation of synapse formation and electrical maturation remains unknown. Considering the mechanical heterogeneity of the developing nervous system[13], we here explored if mechanical signals regulate neuronal maturation. We found a strong dependence of the temporal development of the electrical maturity of neurons on the stiffness of their environment and identified a molecular mechanotransduction pathway linking tissue mechanics to neuronal maturation.

Results

Synaptic density is lower on stiff substrates compared to soft ones

To investigate the effect of substrate stiffness on synapse formation, we cultured primary hippocampal neurons from E17 or E18 rat embryos on soft and stiff polyacrylamide gels coated with Poly-D-Lysine (PDL) and laminin. The shear elastic modulus of *soft* substrates was ~0.1 kPa and that of *stiff* substrates ~10 kPa, corresponding to *in vivo* measurements of soft and stiff brain regions, respectively[19]. After 10 and 14 days of culture (DIV 10 and DIV 14), the cells were fixed and stained for the presynaptic markers vesicular glutamate transporters (VGLUT2) and vesicular GABA transporters (VGAT), the postsynaptic cell adhesion protein neuroligin (NRL), and neurofilaments (NF), which are particularly abundant in axons. Cells were then imaged using confocal laser scanning microscopy (Fig 1a, b) and analysed with a custom synapse density analysis script (see

Methods). Synapses were identified if a pre- and postsynaptic marker co-localised within 2 pixels (360 nm) of each other and the neurofilament marker (Extended Data Figure 1). Synapse densities were determined by dividing the synapse counts by the total length of neurofilaments in each field of view.

The density of both inhibitory GABAergic and excitatory glutamatergic synapses was significantly lower on stiff substrates than on soft substrates at both DIV 10 (Fig 1c) and at DIV 14 (Fig 1d). These results suggested that synapse formation, which is a prerequisite for the establishment of functional neuronal circuits, is more efficient on soft substrates.

Sodium current density is lower on stiff substrates compared to soft ones

The presence of voltage-gated ion channels in the cell membrane is essential for the proper function of mature neuronal circuits. These ion channels contribute to a neuron's excitability, i.e., the likelihood that neurons will fire action potentials in response to stimuli. To explore if substrate stiffness impacted the timing of neuronal electrical excitability, we measured current density - a measure of the electric current flow across the cell membrane - on substrates of different stiffness. Current densities were calculated by normalising the measured currents by the membrane capacitance, which is proportional to the surface area. We focused on three ion channel currents: voltage-gated sodium currents (I_{Na}), voltage-gated potassium currents (I_K), and delayed rectifier potassium currents (I_{Kdr}). Current densities were assessed using whole-cell patch clamp recordings (see Methods) on primary hippocampal neurons at multiple time points during the maturation period up to DIV 14.

The capacitance of the cells increased throughout the duration of the 14-day culture period (between DIV 2 and 14 by a factor of ~4, Extended Data Figure 2), indicating that the neurons kept growing throughout the culture period. Increases in capacitance were similar on both types of

substrates (Extended Data Figure 2), suggesting that, in line with previous observations[20], hippocampal neuronal growth is independent of substrate stiffness.

The I_K and I_{Kdr} densities were not significantly affected by substrate stiffness at any time point (Fig. 1e). At DIV 5, we also did not find an effect of substrate stiffness on I_{Na} densities. However, from DIV 7 to DIV 14, I_{Na} densities were significantly higher in neurons grown on soft substrates (Fig. 1e), suggesting that voltage gated sodium channels were expressed earlier and maturation happened sooner in neurons grown on softer substrates.

Spontaneous and evoked APs are delayed on stiff substrates

Neurons communicate via action potentials, which are rapid changes in the voltage across their membrane. The initial rapid rise in potential ('depolarization') is initiated by the opening of sodium ion channels in the plasma membrane. Since the voltage-gated sodium current density was lower in neurons cultured on stiff substrates, substrate stiffness could potentially affect the generation of action potentials and the formation of functional neuronal circuits.

To test this hypothesis, we investigated if substrate stiffness affected the ability of neurons to generate spontaneous and evoked action potentials over a 14-day culture period. Spontaneous action potentials occur in neurons in the absence of external stimuli and are commonly observed during healthy neuronal and network maturation[21]. Evoked action potentials, on the other hand, are generated in response to experimental stimuli, typically through current injection.

Neurons grown on soft substrates began generating spontaneous action potentials as early as DIV 5, whereas neurons on stiff substrates only started spontaneous firing at DIV 10 (Fig. 1f). These results indicated that the onset of spontaneous action potential activity was delayed in neurons grown on stiffer substrates, and neurons on softer substrates matured more rapidly, in about half the time. By DIV 10, neurons on stiff substrates caught up and showed a comparable proportion of electrically active cells (~50%, Fig. 1f).

We observed a similar delay in the onset of evoked action potential activity in neurons grown on stiff substrates (Fig. 1g). On soft substrates, the proportion of cells capable of generating evoked action potentials increased four-fold throughout the progression of the culture period, from 20% at DIV 5 to 80% at DIV 14, suggesting increased neuronal excitability from DIV 5. In contrast, on stiff substrates, although we observed a small proportion of excitable cells at 4 DIV, none of the cells recorded at DIV 5 and DIV 7 could be induced to fire action potentials. From DIV 10 onwards, we found cells capable of firing evoked action potentials on stiff substrates, but fewer compared to cells on soft substrates at the same time points (Fig. 1g). Together with our data on synapse formation (Fig. 1a-d), sodium current densities (Fig. 1e), and spontaneous neuronal activity (Fig. 1f), these data indicated a delay in neuronal maturation of on stiff substrates.

Substrate stiffness-dependence of neuronal activity is mediated by Piezo1

We next investigated the molecular mechanism underlying the neuronal responses to substrate stiffness ('mechanotransduction'). Since the mechanosensitive ion channel, Piezo1, is expressed in neurons[14,22] and activated in a substrate stiffness-dependent manner at least in fibroblasts[23], we established two independent CRISPR-Cas9 assays to downregulate the expression of Piezo1 in primary hippocampal neurons. Each knockdown (KD) condition (P1 KD1 and P1 KD2) was modified with 4 different guides designed to target different regions in the *Piezo1* gene, while the control (CTRL) was treated with Cas9 protein and CRISPR RNA only (Methods, Extended Data Fig. 3, 4, 5). Having established the timing of neuronal maturation on soft and stiff substrates (Fig. 1), we now tested the effect of Piezo1 knockdown on the activity of neurons cultured on soft and stiff substrates at DIV 5, 6 and 7 using calcium imaging. Data were analysed with a custom-written automated script that detected calcium transients with a sensitivity of 96% and a specificity of 98% (Fig. 2 a-c, Extended Data Figs. 6, 7. See Methods for details).

At DIV 5, we did not detect any significant activity in any of the conditions. Consistent with our previous experiments, in the control condition from DIV 6 onwards, the fraction of active cells was significantly higher on soft substrates than on stiff ones (Fig. 2 d, e, g; Supplementary Information Videos 1, 2). In fact, while the fraction of active cells increased steadily on soft substrates, barely any cells showed any activity on stiff substrates. Inhibition of fast voltage-gated sodium channels and thus action potentials with tetrodotoxin (TTX) resulted in a suppression of calcium signals, indicating that the observed calcium peaks were specific to neuronal electrical activity (Extended Data Fig. 8).

Knockdown of Piezo1 led to a significant increase in the activity of neurons cultured on stiff substrates starting from DIV 6 (Fig. 2 f, g; Supplementary Information Videos 3, 4). The activity of neurons cultured on soft substrates, on the other hand, was not significantly altered by the Piezo1 knockdown. The fraction of KD cells showing calcium transients on stiff substrates was similar to that of CTRL neurons cultured on soft substrates (Extended Data Fig. 9). These data suggested that an enhanced Piezo1 activity on stiff substrates delayed the electrical maturation of neurons, while Piezo1 knockdown abrogated this delay.

Piezo1 regulates substrate stiffness-dependent GABAR and GLUR1 expression via Transthyretin

To determine potential signalling cascades regulating neuronal maturation downstream of Piezo1, we used RNAseq for an unbiased comparison of global alterations in CTRL and Piezo1 KD (P1 KD1 and P1 KD2) neurons cultured on soft vs. stiff substrates at DIV 7 using RNAseq (Fig. 3a). In CTRL cells, 55 genes were significantly differentially regulated (p-value < 0.05, |FoldChange| >=1.1), with 22 genes with differentially increased expression on soft substrates and 33 genes with differentially increased expression on stiff ones.

The RNAseq analysis revealed that the most significantly differentially expressed gene for CTRL neurons cultured on soft and stiff substrates was transthyretin (TTR; $p = 6.6*10^{-5}$; 3.7 fold

higher expression on soft than on stiff) (Fig. 3a), which we confirmed at the protein level using Western blots (Fig. 3c, d). Moreover, TTR's expression pattern resembled the activity pattern of neurons in the different conditions at DIV 7: We found significantly higher expression of TTR and neuronal activity on soft substrates then on stiff ones, and knockdown of Piezo1 led to similarly high TTR expression and electrical activity on soft and stiff substrates (Fig. 3b), indicating a strong relationship between TTR and Piezo1-mediated neuronal maturation.

TTR was originally identified as a thyroxine and retinol transporter[24], and was recently found to also regulate GABA receptor expression[25] and NMDA receptor activation[26], which in turn increases the expression of glutamate receptors of the AMPA family[27] (*cf.* Fig. 3e). As TTR expression was regulated by substrate stiffness (Fig. 3 a-d), we next quantified the substrate stiffness-dependence of the expression of synaptic (GABAergic and glutamatergic) receptors at the protein level using Western blots at DIV 7, focusing on GABA(A) receptors (GABAR), glutamate receptors (GLUR1), and NMDA receptors (NMDAR).

For all replicates, the ratio **r** between the normalised signals from CTRL neurons grown on soft and stiff substrates for the synaptic receptors GLUR1 and GABAR was significantly larger than 1 (Fig. 3d). These results indicated that the expression of these proteins was higher in neurons grown on soft substrates compared with stiff substrates, for all replicates, in line with the expression profile of TTR. The ratio for NMDAR scattered around 1, indicating no dependence of its expression levels on substrate stiffness.

Our results suggested that stiff substrates activate Piezo1, which then suppresses the expression of TTR, leading to delayed neuronal maturation (Fig. 3e). To confirm a role of TTR downstream of Piezo1, we knocked down TTR expression in neurons and used calcium imaging to determine the fraction of active cells on soft and stiff substrates at DIV 7 (Extended Data Fig. 10, Methods). In agreement with an inhibitory role of Piezo1 activity on TTR expression levels, the fraction of active TTR KD cells cultured on soft substrates was as low as that of CTRL neurons

cultured on stiff substrates (Fig. 3 f), confirming a direct link between substrate stiffness, Piezo1 activity, TTR expression levels and neuronal maturation *in vitro*.

Synapse formation *in vivo* is regulated by tissue stiffness

We then investigated if tissue stiffness regulates neuronal maturation *in vivo*, by perturbing brain tissue stiffness in developing *Xenopus laevis* embryos and studying synapse formation. To increase brain tissue stiffness, we applied transglutaminase (TG), an enzyme that cross-links extracellular matrix (ECM) proteins. In the developing mouse brain, TG expression is enhanced in the neurogenic niche, which is stiffer than the non-neurogenic brain parenchyma[28], and TG application in heart tissues leads to tissue stiffening[29].

The application of TG to exposed brains of stage 33-34 *Xenopus* embryos for two hours led to a significant stiffening of the tissue *in vivo* as assessed by atomic force microscopy[14,15] at stage 35-36 (Fig. 4a, b). As stiffer substrates slowed down neuronal maturation *in vitro*, we tested if *in vivo* synapse formation was also delayed in stiffer brains.

From stage 37-38 onwards, brains of wild type animals showed a characteristic pattern of synapses (visualised by FM1-43 fluorescence, which allows the visualization of synaptic vesicle recycling in living cells), including a semicircle surrounding the telencephalon (Fig. 4a, c) coinciding with the position of the supraoptic tract[30] (Extended Data Fig. 11). In contrast, in TG-treated, stiffened brains, these patterns were mostly absent at the same stage (Fig. 4d). Quantification of fluorescence intensity line profiles across this region confirmed significant differences between control and stiffened brains (Fig. 4e-g), indicating fewer synapses in this region in stiffened brains. Immunohistochemistry of acetylated tubulin, an axonal marker, revealed that axon tracts formed normally in both conditions (Extended Data Fig. 12), suggesting that the lower number of synapses in the stiffened brains was indeed a consequence of a delay in maturation rather than perturbed axon growth.

To corroborate this hypothesis, stage 37 embryos were transferred to *Xenopus* recovery media (Supplementary Information Methods 1) and left to develop for another 8 hours until stage 39. Post recovery, both groups displayed similar patterns of FM1-43 fluorescence (Fig. 4 h, i) and peaks in their intensity profiles (Fig. 4j-l), indicating that synapses had now formed, and thus confirming that the stiffening of the brains indeed delayed synapse formation *in vivo*.

Discussion

Here we have shown that the electrical maturation of neurons is regulated by environmental stiffness. The electrical activity, neurotransmitter receptors and synapses of primary neurons developed faster in softer environments than in stiffer ones. Knockdown of the mechanosensitive ion channel Piezo1 abolished the delay in neuronal maturation on stiff substrates. We identified Transthyretin (TTR) as a key player in regulating neuronal maturation downstream of Piezo1. On soft substrates, TTR expression levels were higher than on stiff substrates, leading to higher expression of GABAR and GLUR1 and earlier electrical maturation (Fig. 3e). Knockdown of Piezo1 resulted in an increase in TTR levels on stiff substrates, which was accompanied by an increase in electrical neuronal activity.

Neuronal growth cones exert higher traction forces and tension on their axon on stiffer substrates than on softer ones[20,31,32]. In fibroblasts, traction forces scale with Piezo1 activity[23], suggesting that the activity of Piezo1 is also higher in axons grown on stiffer substrates. Our data indicate that this increased activity of the mechanosensitive ion channel on stiff substrates leads to a downregulation of TTR, thus slowing down neuronal maturation.

How Piezo1 activity leads to a decrease in TTR remains to be studied. As a non-selective cation channel, Piezo1 activation gives rise to calcium transients. Piezo1-medicated calcium influxes on stiffer substrates could activate calcium-dependent signalling cascades, potentially leading, for example, to the phosphorylation of repressive transcription factors and subsequent

downregulation of TTR expression. Alternatively, Piezo1 activity could lead to an activation of the PI3K/Akt pathway[33], which antagonizes TTR activity by inhibition of GSK3[34]. The subsequent downregulation of both GABAergic and glutamatergic receptors explains the delay in synapse formation on stiff substrates and in stiffened *Xenopus laevis* brain tissue.

The regulation of the electrical maturation of neurons by brain stiffness has major implications for brain development, given that some brain regions are softer than others[14], and local brain tissue stiffness changes during development[15,35–37] and in neurodevelopmental disorders[38]. Our study indicates that local brain tissue stiffness regulates the onset and rate of electrical maturation in each brain area and at different developmental time points, thereby potentially establishing the foundation for the emergence of the first circuits in the developing brain.

Brain tissue stiffness is determined by multiple factors, including the stiffness, density and connectivity of the cells found in the area and the composition of the ECM[39,13]. Alterations in any of these components may thus impact neuronal maturation during brain development. Similarly, impaired mechanosensitivity, for instance through altered expression levels or mutations of mechanosensitive proteins, might affect the maturation speed of neurons and consequently alter the emerging circuitry. Knowledge about when and where the regulation of neuronal maturation by tissue stiffness is critical during brain development will help understanding the emergence of healthy neural circuitry and potentially also the onset of different neurodevelopmental disorders, and it may contribute to a better understanding of the decline in neuronal function in the ageing brain, whose mechanical properties change with age and in neurodegenerative diseases[13].

References

1. Alvarez-Dominguez, J. R. & Melton, D. A. Cell maturation: Hallmarks, triggers, and manipulation. *Cell* **185**, 235–249 (2022).
2. Wallace, J. L. & Pollen, A. A. Human neuronal maturation comes of age: cellular mechanisms and species differences. *Nat. Rev. Neurosci.* **25**, 7–29 (2024).
3. Spitzer, N. C. Electrical activity in early neuronal development. *Nature* **444**, 707–712 (2006).
4. Park, H. & Poo, M. Neurotrophin regulation of neural circuit development and function. *Nat. Rev. Neurosci.* **14**, 7–23 (2013).
5. Shen, K. & Cowan, C. W. Guidance Molecules in Synapse Formation and Plasticity. *Cold Spring Harb. Perspect. Biol.* **2**, a001842 (2010).
6. Chen, S.-Y. & Cheng, H.-J. Functions of axon guidance molecules in synapse formation. *Curr. Opin. Neurobiol.* **19**, 471–478 (2009).
7. Bando, Y., Ishibashi, M., Yamagishi, S., Fukuda, A. & Sato, K. Orchestration of Ion Channels and Transporters in Neocortical Development and Neurological Disorders. *Front. Neurosci.* **16**, 827284 (2022).
8. Desarmenien, M. G. & Spitzer, N. C. Role of calcium and protein kinase C in development of the delayed rectifier potassium current in xenopus spinal neurons. *Neuron* **7**, 797–805 (1991).
9. Ciceri, G. *et al.* An epigenetic barrier sets the timing of human neuronal maturation. *Nature* **626**, 881–890 (2024).
10. Moore, A. R. *et al.* Electrical Excitability of Early Neurons in the Human Cerebral Cortex during the Second Trimester of Gestation. *Cereb. Cortex* **19**, 1795–1805 (2009).
11. Bradke, F., Di Giovanni, S. & Fawcett, J. Neuronal Maturation: Challenges and Opportunities in a Nascent Field. *Trends Neurosci.* **43**, 360–362 (2020).

12. Ronaldson-Bouchard, K. *et al.* Advanced maturation of human cardiac tissue grown from pluripotent stem cells. *Nature* **556**, 239–243 (2018).

13. Pillai, E. K. & Franze, K. Mechanics in the nervous system: From development to disease. *Neuron* **112**, 342–361 (2024).

14. Koser, D. E. *et al.* Mechanosensing is critical for axon growth in the developing brain. *Nat. Neurosci.* **19**, 1592–1598 (2016).

15. Thompson, A. J. *et al.* Rapid changes in tissue mechanics regulate cell behaviour in the developing embryonic brain. *eLife* **8**, (2019).

16. Previtera, M. L., Langhammer, C. G., Langrana, N. A. & Firestein, B. L. Regulation of Dendrite Arborization by Substrate Stiffness is Mediated by Glutamate Receptors. *Ann. Biomed. Eng.* **38**, 3733–3743 (2010).

17. Flanagan, L. A., Ju, Y.-E., Marg, B., Osterfield, M. & Janmey, P. A. Neurite branching on deformable substrates. *Neuroreport* **13**, 2411–2415 (2002).

18. Zhang, Q.-Y. *et al.* Stiff substrates enhance cultured neuronal network activity. *Sci. Rep.* **4**, 6215 (2014).

19. Franze, K., Janmey, P. A. & Guck, J. Mechanics in Neuronal Development and Repair. *Annu. Rev. Biomed. Eng.* **15**, 227–251 (2013).

20. Koch, D., Rosoff, W. J., Jiang, J., Geller, H. M. & Urbach, J. S. Strength in the Periphery: Growth Cone Biomechanics and Substrate Rigidity Response in Peripheral and Central Nervous System Neurons. *Biophys. J.* **102**, 452–460 (2012).

21. Raman, I. M. & Bean, B. P. Ionic Currents Underlying Spontaneous Action Potentials in Isolated Cerebellar Purkinje Neurons. *J. Neurosci.* **19**, 1663–1674 (1999).

22. Pathak, M. M. *et al.* Stretch-activated ion channel Piezo1 directs lineage choice in human neural stem cells. *Proc. Natl. Acad. Sci.* **111**, 16148–16153 (2014).

23. Ellefsen, K. L. *et al.* Myosin-II mediated traction forces evoke localized Piezo1-dependent Ca 2+ flickers. *Commun. Biol.* **2**, 1–13 (2019).

24. Vieira, M. & Saraiva, M. J. Transthyretin: a multifaceted protein. *Biomol. Concepts* **5**, 45–54 (2014).

25. Zhou, L. *et al.* Identification of transthyretin as a novel interacting partner for the δ subunit of GABAA receptors. *PLoS ONE* **14**, (2019).

26. Gomes, J. R. *et al.* Transthyretin provides trophic support via megalin by promoting neurite outgrowth and neuroprotection in cerebral ischemia. *Cell Death Differ.* **23**, 1749–1764 (2016).

27. O'Brien, R. J. *et al.* Activity-Dependent Modulation of Synaptic AMPA Receptor Accumulation. *Neuron* **21**, 1067–1078 (1998).

28. Kjell, J. *et al.* Defining the Adult Neural Stem Cell Niche Proteome Identifies Key Regulators of Adult Neurogenesis. *Cell Stem Cell* **26**, 277-293.e8 (2020).

29. Majkut, S. *et al.* Heart-Specific Stiffening in Early Embryos Parallels Matrix and Myosin Expression to Optimize Beating. *Curr. Biol.* **23**, 2434–2439 (2013).

30. Anderson, R. B. & Key, B. Novel guidance cues during neuronal pathfinding in the early scaffold of axon tracts in the rostral brain. *Development* **126**, 1859–1868 (1999).

31. Franze, K. Integrating Chemistry and Mechanics: The Forces Driving Axon Growth. *Annu. Rev. Cell Dev. Biol.* **36**, 61–83 (2020).

32. Kreysing, E. *et al.* Effective cell membrane tension is independent of polyacrylamide substrate stiffness. *PNAS Nexus* **2**, pgac299 (2023).

33. Chen, P. *et al.* Mechanosensitive Piezo1 in endothelial cells promotes angiogenesis to support bone fracture repair. *Cell Calcium* **97**, 102431 (2021).

34. Zawiślak, A., Jakimowicz, P., McCubrey, J. A. & Rakus, D. Neuron-derived transthyretin modulates astrocytic glycolysis in hormone-independent manner. *Oncotarget* **8**, 106625–106638 (2017).

35. Elkin, B. S., Ilankovan, A. & Morrison, B., III. Age-Dependent Regional Mechanical Properties of the Rat Hippocampus and Cortex. *J. Biomech. Eng.* **132**, (2009).

36. Iwashita, M., Kataoka, N., Toida, K. & Kosodo, Y. Systematic profiling of spatiotemporal tissue and cellular stiffness in the developing brain. *Development* **141**, 3793–3798 (2014).

37. Ryu, Y., Iwashita, M., Lee, W., Uchimura, K. & Kosodo, Y. A Shift in Tissue Stiffness During Hippocampal Maturation Correlates to the Pattern of Neurogenesis and Composition of the Extracellular Matrix. *Front. Aging Neurosci.* **13**, (2021).

38. McIlvain, G. *et al.* Brain Stiffness Relates to Dynamic Balance Reactions in Children with Cerebral Palsy. *J. Child Neurol.* **35**, 463–471 (2020).

39. Long, K. R. & Huttner, W. B. The Role of the Extracellular Matrix in Neural Progenitor Cell Proliferation and Cortical Folding During Human Neocortex Development. *Front. Cell. Neurosci.* **15**, (2022).

40. Benjamini, Y. & Hochberg, Y. Controlling the False Discovery Rate: A Practical and Powerful Approach to Multiple Testing. *J. R. Stat. Soc. Ser. B Methodol.* **57**, 289–300 (1995).

41. Muresan, L., Jacak, J., Klement, E. P., Hesse, J. & Schutz, G. J. Microarray Analysis at Single-Molecule Resolution. *IEEE Trans. NanoBioscience* **9**, 51–58 (2010).

42. Frangi, A. F., Niessen, W. J., Vincken, K. L. & Viergever, M. A. Multiscale vessel enhancement filtering. in *Medical Image Computing and Computer-Assisted Intervention — MICCAI'98* (eds. Wells, W. M., Colchester, A. & Delp, S.) 130–137 (Springer, Berlin, Heidelberg, 1998). doi:10.1007/BFb0056195.

43. Qin, X. *et al.* U^2-Net: Going Deeper with Nested U-Structure for Salient Object Detection. *Pattern Recognit.* **106**, 107404 (2020).

44. S. Andrews. FastQC: A Quality Control Tool for High Throughput Sequence Data. (2010).

45. Babraham Bioinformatics - Trim Galore! https://www.bioinformatics.babraham.ac.uk/projects/trim_galore/.

46. Dobin, A. *et al.* STAR: ultrafast universal RNA-seq aligner. *Bioinformatics* **29**, 15–21 (2013).

47. Anders, S., Pyl, P. T. & Huber, W. HTSeq—a Python framework to work with high-throughput sequencing data. *Bioinformatics* **31**, 166–169 (2015).

48. Love, M. I., Huber, W. & Anders, S. Moderated estimation of fold change and dispersion for RNA-seq data with DESeq2. *Genome Biol.* **15**, 550 (2014).

49. Nieuwkoop, P. D. & Faber, J. *Normal Table of Xenopus Laevis (Daudin): A Systematical and Chronological Survey of the Development from the Fertilized Egg till the End of Metamorphosis*. (North-Holland Pub. Co., 1967).

Figures

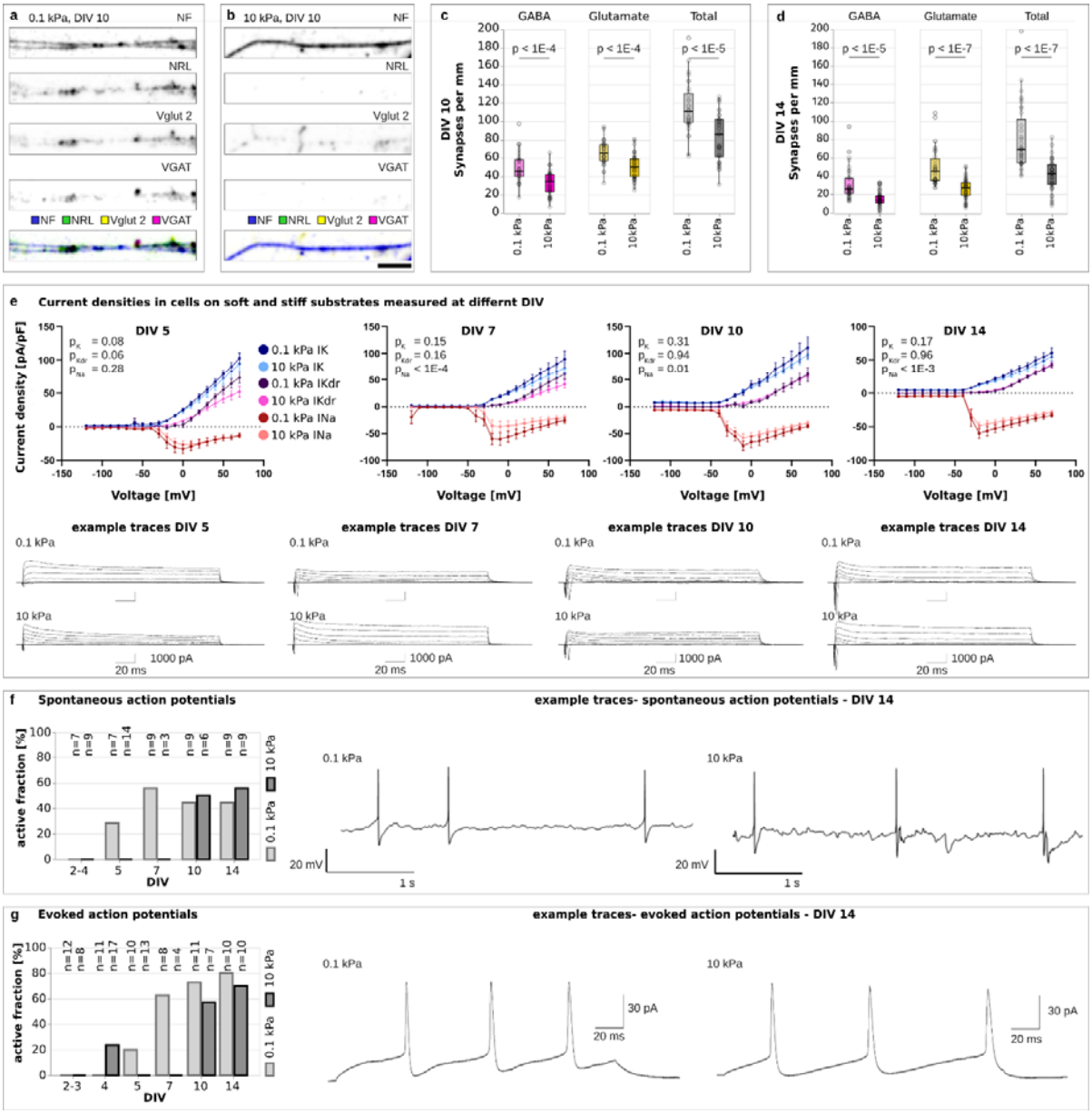

Figure 1 | Synapse densities and neuronal activity are lower on stiff substrates than on soft substrates. (a, b) Immunocytochemistry of neurons cultured on (a) soft (0.1 kPa) and (b) stiff (10 kPa) substrates, showing (from top to bottom) neurofilament (NF), postsynaptic marker (NRL), vesicular glutamate transporter 2 (Vglut 2; excitatory), vesicular GABA transporter (VGAT; inhibitory), and an overlay of all channels. (c,d) Quantification of synapse densities. Both glutamatergic and GABAergic synapse densities were lower on stiff substrates than on soft ones at

DIVs 10 and 14. Box plots showing detected synapses per mm neurofilament; *p*-values provided above the plots (two-tailed t-tests). (e) Current densities for voltage-gated sodium (I_{Na}) and potassium (I_K, I_{Kdr}) channels assessed by whole cell patch clamp recordings at different time points. Sodium current densities were significantly higher on soft substrates than on stiff ones from DIV 7 to DIV 10/14 (two-way ANOVA followed by Sidak's multiple comparisons test). Representative traces are shown below. (f) Whole cell patch clamp experiments were performed to detect spontaneous action potentials (APs). On soft gels, spontaneous APs were detected from DIV 5 until the end of the culture period, whilst neurons on stiff gels did not show any spontaneous activity until DIV 10. At DIVs 10 and 14, cells showed similar levels of activity regardless of the environmental stiffness, suggesting that the electrical maturation of neurons is delayed on stiffer substrates. Representative traces of spontaneous activity are from cells at DIV 14. (g) Evoked action potentials measured by whole cell patch clamp experiments. On soft gels, the proportion of neurons with inducible action potentials increased throughout the culture period, while on stiff gels, with the exception of DIV 4, action potentials were inducible from DIV 10. Representative traces were taken at DIV 14. Scale bar: 5 µm.

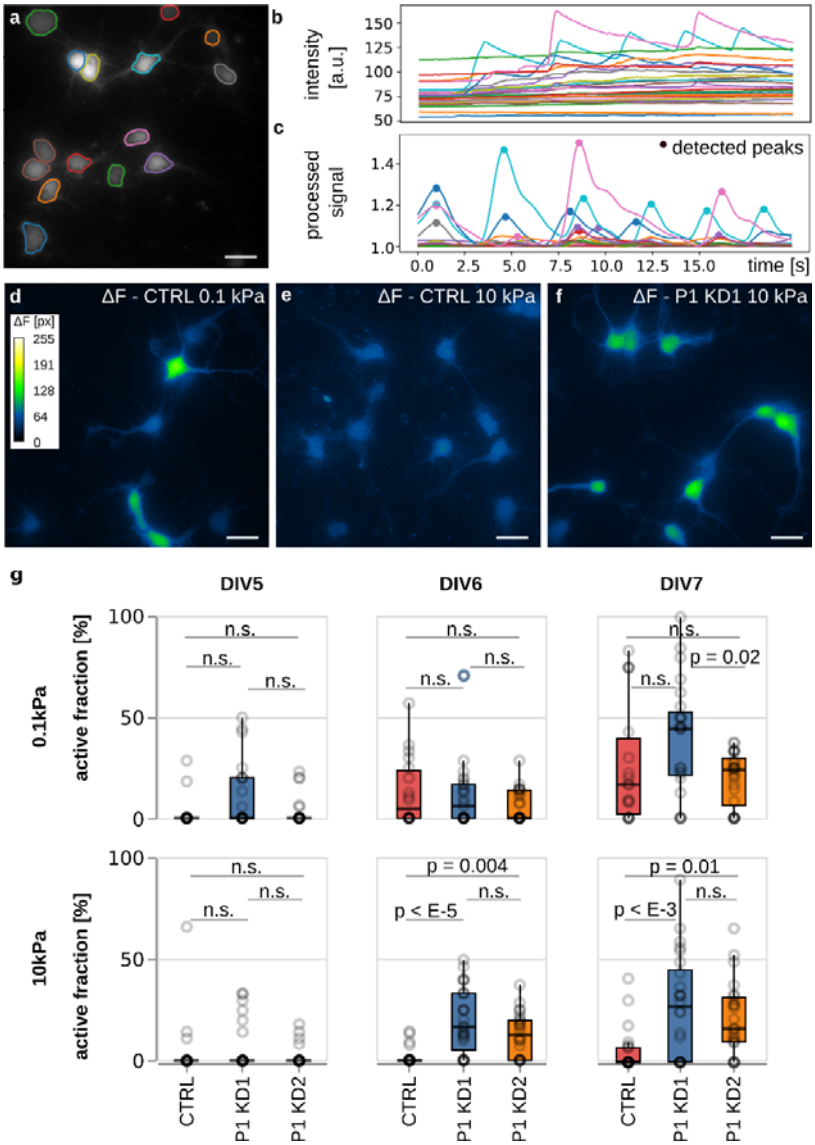

Figure 2: Piezo1 delays electrical maturation of neurons on soft substrates. (a) Image of neurons incubated with the calcium indicator Rhod-4, outlines of somata were determined semi-automatically, and averaged fluorescence intensities of each region of interest (ROI) calculated. (b) Plot of the baseline-corrected averaged intensity of each cell as a function of time. (c) Plot of processed signals with automatically detected intensity peaks. (d-f) Images showing the intensity variation ΔF detected over 40 seconds; the change in fluorescence intensity over time is colour-coded. CTRL cells on (d) soft substrates showed strong intensity variability, whereas (e) on stiff substrates intensity fluctuations were very low, indicating little neuronal activity. (f) Knockdown of Piezo1 rescued the spontaneous activity of neurons on stiff gels. (g) Plots of the fraction of active

cells as a function of substrate stiffness and time (n=3546 cells from 418 fields of view). CTRL neurons (red) on soft substrates became active at DIV 6, whereas those on stiff substrates did not show any substantial activity yet at DIV 7. Knockdown of Piezo1 (blue and yellow) led to a significant increase in activity of neurons cultured on stiff substrates from DIV 6 (Kruskal-Wallis test followed by a Tukey posthoc test), indicating that Piezo1 activity delayed the electrical activity of neurons on stiff substrates. Scale bars: 25 µm. See also Supplementary Information Video 1-4.

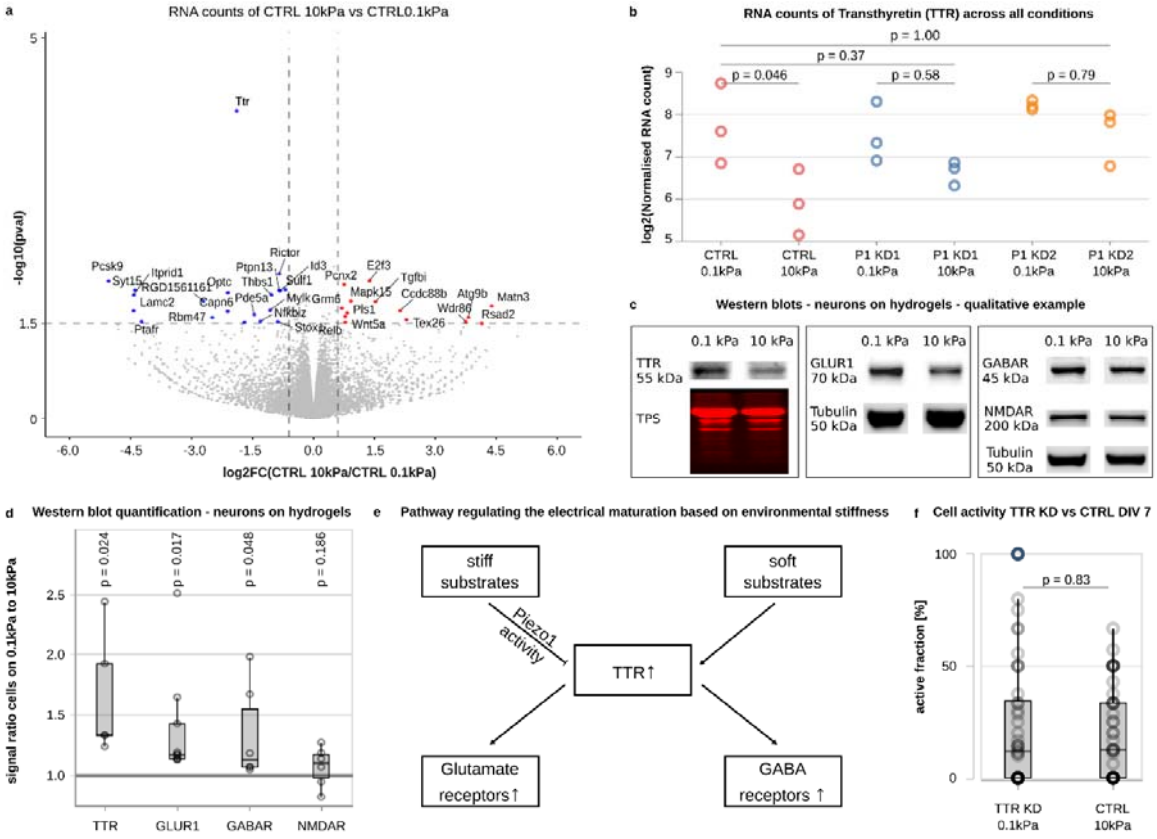

Figure 3: Transthyretin (TTR) regulates electrical maturation of neurons downstream of Piezo1. (a) Volcano plot of RNA sequencing results of CTRL neurons grown on soft *vs.* stiff substrates at DIV 7. Fold change is shown on x (blue: higher expression on soft, red: higher expression on stiff gels), p-values on y. The most significant change between the conditions occurred in the expression of TTR. (b) TTR RNA counts normalised by sample-specific size factors for CTRL and Piezo1 knockdown neurons on soft and stiff substrates as assessed by RNA sequencing. The pattern of TTR expression in the different groups resembled that of their activity at DIV 7 (low in CTRL neurons cultured on stiff substrates, high in all other conditions; Fig. 2g), suggesting a link between TTR levels and neuronal maturation (ANOVA test followed by a Tukey posthoc test). (c) Representative Western blots of CTRL neurons cultured on soft and stiff substrates at DIV 7, stained for TTR, glutamate 1 receptors (GLUR1), GABA receptors (GABAR), and NMDA receptors (NMDAR). (d) Analysis of Western blots of CTRL neurons cultured on soft and stiff substrates at DIV 7. The expression of TTR, GLUR1, and GABAR was significantly higher on soft

than on stiff substrates, whereas NMDAR expression was similar in both conditions (n=320 WB bands from 3 biological replicates; one-sided 1-sample t-test). (e) Proposed pathway linking Piezo1 activity with the expression of TTR and, secondarily, synaptic receptors, suggesting a potential mechanism for the delay in electrical maturation of neurons on stiff substrates. (f) Plot of the fraction of active cells in TTR KD neurons on soft substrates and CTRL neurons on stiff substrates assessed by calcium imaging. No significant differences were found, supporting the proposed model shown in (e) (n=44 CTRL cells and 41 TTR KD cells; Mann-Whitney test).

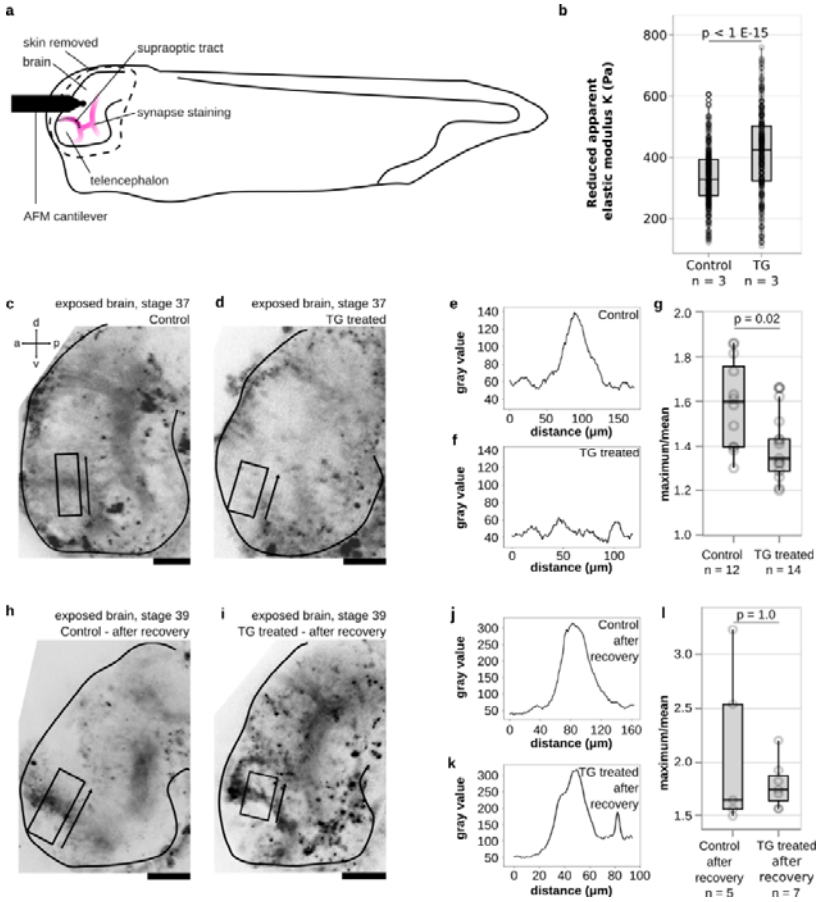

Figure 4: Synapse formation is delayed in stiffened brain tissue *in vivo*. (a) Schematic of a *Xenopus laevis* embryo whose brain was exposed, enabling stiffness measurements by AFM and fluorescence imaging of functional synapses (indicated in pink). (b) Plot of apparent elastic moduli of *in vivo Xenopus laevis* brain tissue measured by AFM. TG treatment led to a significant stiffening of the tissue (two-tailed t-test). (c-d, h-i) Images of exposed *Xenopus laevis* brains; synapses were stained using FM1-43. (c) At stage 37, a typical staining pattern is found in control embryos in the area of the supraoptic tract. (d) In stiffened brains, this pattern was largely absent. (e, f) Intensity profiles along the stripes indicated in (c, d). While the untreated brain showed a strong peak, the TG profile was noise-dominated. (g) Plot of the ratio of the maximum over the mean value in each profile, which was significantly higher in control brains (Mann-Whitney test), indicating more functional synapses in the control animals. (h, i) After a recovery period of 8 hours, strong signals in the area of the supraoptic tract were visible in either condition, suggesting that synapse

formation was delayed in the stiffened brains. (j, k) Line profiles show very similar features between the two conditions at stage 39. (l) The ratio of the maximum value over the mean value showed no significant difference at stage 39 (Mann-Whitney test). Scale bars:100 µm.

Methods

Preparation and coating of hydrogels

Hydroxy-polyacrylamide substrates were fabricated as described in[14]. Glass bottom Petri dishes as well as glass coverslips with 18 mm diameter were washed in 70% ethanol, followed by distilled water and then air dried. The glass bottoms were wiped with 1M NaOH, allowed to dry and incubated for 3 min with (3-aminopropyl)trimethoxysilane (APTMS, Sigma Aldrich, 281778). APTMS was then washed off and the glass bottoms were incubated with 0.5% glutaraldehyde for 30 min. The glass bottoms were then washed three times with distilled water. The coverslips were incubated with Rain-X (Shell Car Care International) for 10 min. To make the acrylamide (AA, Sigma Aldrich, A4058) stock solution, 500 µl of 40% acrylamide was mixed with 65 µL of 100% hydroxyacrylamide (Sigma Aldrich, 697931). To prepare the gel premix, 500 µl of acrylamide stock solution was mixed with 250 µl of 2% bis-acrylamide (BA, Fisher Scientific, BP1404-250). For 0.1 kPa hydrogels, 53 µl of the premix was diluted with 447 µl PBS, and for 10 kPa hydrogels, 150 µl was diluted with 350 µl PBS. These mixtures were then placed in a vacuum chamber for 4-6 min. Then, 1.5 µL of 0.3% (v/v) N,N,N′,N′-tetramethylethylenediamine (TEMED, Thermo Fisher, 15524–010) and 5 µL of 0.1% (w/v) ammonium persulfate (APS, Sigma, 215589) solution were added to the gels and mixed. Next, 14 µL of the gel mixture was pipetted onto each glass bottom and covered with a RainX-treated coverslip. The dishes were then filled with 2 mL PBS and left for 20 min before the coverslips were removed. The gels were washed twice with sterile PBS in a tissue culture hood, treated with UV light for 30 min and washed again with PBS. Subsequently, the gels were coated with 10-50 µg/ml PDL in PBS overnight at 4°C, washed three times with PBS, and finally coated with 1-2 µg/ml laminin in Neurobasal media (NB media, Gibco) with 2% PSF at 37°C for 4 hours.

Tissue dissection

All rat dissections were conducted in compliance with the Ethical Review Committee of the University of Cambridge and the UK Home Office.

Pregnant Charles River Sprague Dawley rats were sacrificed at E17 or E18. They were anaesthetised with 5% isoflurane before cervical dislocation and exsanguination. The uteri were removed and transferred into a sterile 100 mm culture dish. The dish was transferred to a sterile horizontal flow hood. The embryonic sacs were opened in a new dish and the embryos transferred into a separate sterile dish. The embryos were decapitated with a razor blade and the heads transferred to a fresh dish with chilled HBSS+ (HBSS w/o Ca, w/o Mg (Gibco) with 2% penicillin-streptomycin-amphotericin B (PSF; Lonza) and kept on an ice pack. The skulls were opened from the neck to the forehead and the brains removed with curved forceps. The brains were moved into a dish containing chilled Hibernate E+ (Hibernate E (Gibco)) with 2% PSF) and kept on an ice pack. Meninges were removed and the hippocampi cut out. The hippocampi were collected in 2ml Eppendorf tubes containing Hibernate E+ and kept in a cooling rack until the dissection was completed.

Neuronal culture

For Patch Clamp and synapse staining experiments, hippocampal tissue was washed in HBSS with 2% PSF, and then incubated with Papain solution for 30 min at 37 °C. The solution was removed and 1ml Ovomucoid was added to stop the papain digestion (Supplementary Information Methods 1). The step was repeated before gentle trituration with a 1 mL pipette. The cell suspension was topped up to 8 ml with Ovomucoid before centrifugation at 1000 RPM for 8 min. The supernatant was removed, and the cells suspended in 1 ml neuron culture medium (Supplementary Information Methods 1). After 24h, half the volume of the media was replaced. Afterwards, half the volume of the media was replaced every 2/3 days.

For wild type (WT) cell culture, hippocampal tissue was washed 3x with cold HBSS+. The buffer was removed and replaced with 2 ml 0.05% prewarmed Trypsin-EDTA (Gibco) and incubated for 10 min at 37°C. The tissue was washed 10x with warm HBSS+.

The HBBS+ was then replaced with 1ml warm Neurobasal complete media (Supplementary Information Methods 1) . Cells were isolated by gently pipetting up and down until most tissue bits were broken down. 150 000 cells were plated per dish in 1.5 ml Neurobasal complete. After 6-12 h, the media was replaced completely. Afterwards, half the volume of the media was replaced every 3 days.

For CRISPR knockdown (KD) and control cells, the CRISPR reagents were prepared before washing the tissue.

For the Piezo1 KD cells, two different sets of guides were prepared. Each set contained 4 different guides that are specific to different regions of the gene (see below). As a control, TRACR RNA was used.

120 pmol of each single-guide RNA (IDT) was incubated with 52 pmol HiFi Cas9 (IDT) in 2.1 µl nuclease-free buffer (IDT) and incubated for 10-20 min at room temperature. Per condition, the 4 specific guide mixes were transferred into 100 µl of electroporation buffer (82 µl electroporation buffer + 18 µl supplement from the Lonza rat nucleofector kit). Additionally, 400 pmol electroporation enhancer (IDT) were added.

For the control cells, 240 pmol of the TRACR RNA (IDT) were incubated with 208 pmol HiFi Cas9 (IDT) in 4.2 µl nuclease-free buffer (IDT) and incubated for 10-20 min. This mixture was transferred into 100 µl of electroporation buffer and 400 pmol electroporation enhancer (IDT) were added.

For the TTR KD cells, two guides were designed (the gene is very short and thus very few target regions were available in the gene). 120 pmol of each single-guide RNA (IDT) was incubated with 104 pmol HiFi Cas9 (IDT) in 2.1 µl nuclease-free buffer (IDT) and incubated for 10-20 min and

then transferred into 100 µl of electroporation buffer and 400 pmol electroporation enhancer (IDT) were added.

For each condition, hippocampal tissue was washed 3x with cold HBSS+. The buffer was removed and replaced with 2 ml 0.05% prewarmed Trypsin-EDTA (Gibco) and incubated for 10 min at 37°C. The tissue was washed 10x with warm HBSS+. Then, the tissue was transferred into the electroporation mix and the cells were isolated by gentle pipetting. The cell suspension was transferred into the electroporation cuvette (Lonza rat nucleofector kit) while avoiding bubbles. The cuvette was placed in the nucleofector 2b (Lonza) and the program O-003 was executed. The cuvette was immediately topped up with 1 ml prewarmed Neurobasal complete media. The content of the cuvette was transferred into a 1.5 ml Eppendorf tube and the cells were counted and plated as described above.

CRISPR guide design and characterisation

Piezo1 KD guides

Two distinct CRISPR-CAS9 knockdown (KD) conditions were established. Each condition was based on four different guides. The eight guides were distributed into sets 1 and 2 in alternating order along the gene (set 1: #1, #3, #5, #7; set 2: #2, #4, #6, #8, see below).

To estimate the editing efficiency of the CRISPR-Cas9 guides used, one guide per set was selected (guide 7 for set 1 and guide 8 for set 2) and the DNA of the experimental and control conditions around the guide of interest were sequenced.

DNA from the control and experimental conditions was extracted and amplified using TOPO cloning. Finally, several bacterial colonies were picked, each containing only a single sequence. The DNA from each colony was extracted and sequenced using Sanger sequencing.

For set 1, DNA from 8 colonies was sequenced containing DNA from the control condition and from 15 colonies from the experimental condition. 5 of the control sequences were mutation

free, 3 sequences could not be used as they only contained the sequence of the cloning vector. Out of 15 sequences obtained from KD set 1, we found 4x point mutation, 9x mutation free, and 2 sequences could not be used as they only contained the sequence of the cloning vector (31% editing).

For set 2, DNA from 4 colonies was sequenced containing DNA from the control condition and from 10 colonies from the experimental condition. The control sequences were all mutation free. Out of 10 sequences obtained from KD set 2, we found 1x point mutation, 1x 7 base mutation, 1x deletion, 7x mutation free (30% editing).

Assuming that all 8 guides have similar editing efficiencies (P_{mut}=0.3), and in each set, 4 guides act independently, the probability of not finding any mutations corresponds to $P_{WT} = (0.7)^4 = 0.24 = 24\%$ (see Extended Data Fig. 5). This suggests a probability of finding at least one mutation in the Piezo1 protein with a probability of P_{mut}= 1-0.24 = 0.76 = 76%.

Given that no two mutations we found in the sequences were the same, we assume an accumulation of random point mutations and occasional frameshifts in the *Piezo1* gene. While the frameshifts lead to lower expression levels of Piezo1, the point mutations lead to changes in amino acids which might change the functionality of the mechosensitive protein e.g. through changes in folding.

Guide sequences were as follows. Set 1 used odd numbered guides, set 2 used even numbered guides:

- #1 GTTGAGACACGTTTGCCCAA (PAM: AGG, exon: 4)
- #2 ACGCTTCAATGCTCTCTCGT (PAM: TGG, exon: 2)
- #3 TCCTTGTGAGGCGTCCACAG (PAM: AGG, exon: 5)
- #4 CCACCCTGGCAACCAAACGC (PAM: AGG, exon: 6)
- #5 CTTTAACACCCTCTGCGTCA (PAM: AGG, exon: 7)
- #6 GAACACCATCAGGTAGACGC (PAM: TGG, exon: 7)

- #7 GTACTCCAGTAACTGCACCG (PAM: AGG, exon: 19)
- #8 CGATTTTGTAGACCACCAGG (PAM: CGG, exon: 14)

TTR guides

For the TTR KD, one CRISPR-CAS9 KD condition was established. Given the very short gene, two guides were designed. To estimate their editing efficiency, DNA was sequenced in the experimental and control conditions around both sequences of interest as described for the Piezo1 KD cells.

For guide 1, DNA from 9 colonies was sequenced containing DNA from the control condition and from 35 colonies from the experimental condition. Out of the 9 control sequences, 8 were mutation free and 1 sequence could not be used as it only contained the sequence of the cloning vector. Out of 35 sequences obtained from the experimental condition, 34 were mutation free and 1 sequence could not be used as it only contained the sequence of the cloning vector. (0% editing).

For guide 2, DNA from 8 colonies was sequenced containing DNA from the control condition and from 12 colonies from the experimental condition. Out of the 8 control sequences, 6 were mutation free and 2 sequences could not be used as they only contained the sequence of the cloning vector. Out of 12 sequences obtained from the experimental condition, 7 were mutation free, 1 had a point mutation, 1 sequence had an insertion, and 3 sequences could not be used as they only contained the sequence of the cloning vector. (22% editing). KD samples show a lower TTR expression than the CTRL (see Extended Data Fig. 10).

The guide sequences were:

- *TTR* guide #1: AAGAGCCTTCCAGTACGATT (PAM: TGG)
- *TTR* guide #2: GTTTTCACAGCCAATGACTC (PAM: TGG)

Immunocytochemistry of synapses in neuronal cultures and imaging

The samples were fixed with 4% PFA for 10 minutes before being washed. To block and permeabilize the samples, they were incubated for 1 hour in 0.1% Triton X-100 and 10% goat serum in PBS at 21°C. Subsequently, the samples were incubated with the primary antibody overnight at 4°C, followed by incubation with the secondary antibody for 1 hour at 21°C. The primary antibodies used were chicken anti-Neurofilament (abcam, ab4680, 1:1000), rabbit anti-neuroligin (Synaptic Systems #129 213, 1:1000), guinea pig Vglut2 (Synaptic Systems #135 404 1:1000), and mouse VGAT (Synaptic Systems #131 011, 1:750). The secondary antibodies were goat anti-chicken IgY H&L (Alexa Fluor 405, abcam, ab175674, 1:1000), goat anti-rabbit IgG-488 (Life Technologies, A-11034), goat anti-guinea pig IgG-568 (Life Technologies # A-21435), and mouse IgG-647 (Life technology, catalogue number unknown, 1:1000). Images were taken on a confocal microscope (Leica, SP8) with a 63x objective (NA=1.4)

Synapse density analysis of immunocytochemistry images

To analyse synapse density, a custom image analysis code was used. First, a maximum intensity projection was performed for all four channels. Subsequently, spot detection was carried out on the neuroligin, vesicular GABA transporter, and the vesicular glutamate transporter channels. This was achieved by enhancing the bright, circular features using an à trous wavelet transform, which is based on order three B-splines and has three detail levels. As the images consist of a dark background superimposed with bright spots, the majority of the computed wavelet coefficients represent the background and were modelled at each wavelet scale as samples from Gaussian distributions with a mean of 0. The signal pixels appeared as outliers in these wavelet coefficient distributions. The outliers were identified by controlling the false discovery rate at a 1% level[40] across the detail levels. The pixel positions classified as outliers across all scales constitute the support of the signal (the spot representing the molecules). To distinguish

between close molecules with overlapping support, the local maxima of the original image were counted within the computed support (see Extended Data Fig. 2). This approach was inspired by[41].

The Frangi vesselness filter[42] was applied to enhance the images of processes. Segmented images of processes were obtained by applying a similar support computation to the spot detection, based on the wavelet transform. Cell bodies were detected in the same channel using Otsu thresholding and separated from processes through morphological opening. The length of a process in each image was measured by summing all pixels in the resulting processes mask after removing the cell body-related area.

If the distance between a neuronal process (NF filament), GABA or glutamate transporter signals and neuroligin was larger than 2 pixels (360 nm), the signals were excluded. Counts were normalised to the total process length and presented in box plots.

Patch clamp recordings

Whole-cell patch clamp recordings were performed using a Multiclamp 700B amplifier (Molecular Devices) connected to a 16-bit digitiser (Axon Digidata 1440A, Molecular Devices), using a CV-7B headstage (Axon Instruments). The software for data acquisition was pClamp 10 with a sampling rate of 50 kHz and a 10 kHz low-pass filter. Cells were continuously perfused with oxygenated artificial cerebrospinal fluid (ACSF) consisting of 144 mM NaCl, 2.5 mM KCl, 2.5 mM $CaCl_2$, 1 mM NaH_2PO_4, 10 mM HEPES, and 10 mM glucose, with pH adjusted to 7.35 using NaOH. The electrodes were filled with an internal recording solution containing 130mM K-gluconate, 4mM NaCl, 0.5mM $CaCl_2$, 10mM HEPES, 10mM BAPTA, 4mM MgATP, 0.5mM Na_2GTP, and 2mM K-Lucifer yellow, with pH adjusted to 7.3 with KOH and an osmolarity of 295 mOsm. The series resistance ranged from 5-20 MΩ, and the electrode junction potentials (-14 mV) were corrected for.

Upon finding a cell a single -5mV voltage pulse was applied for 50ms to generative cell membrane capacitive transients, so that series resistance, membrane resistance and cell membrane capacitance could be calculated. The time constant of a single exponential curve was fitted to the transients and the cell membrane properties calculated using MATLAB. A voltage step protocol was used to examine ion channels currents. A series of 20 200ms, 10mV voltage steps, from -120mV to +70mV, were applied to the cell and the sodium and potassium current responses recorded. The maximum sodium current (I_{Na}), the maximum potassium current (I_K) and the delayed rectifier potassium current (I_{Kdr}) were detected using a custom MATLAB script. The current densities of the voltage gated ion channel currents were calculated by dividing the resultant current by the cell membrane capacitance. Groups differences were assessed via Two-Way ANOVA followed by Sidak's multiple comparisons test, using GraphPad Prism 10.2.1.

Spontaneous and evoked action potentials were recorded in current clamp recording configuration with a 1kHz sampling frequency. To record spontaneous action potentials baseline current was injected to so that the cell membrane was at -60mV, and gap-free recording carried out for up to 10 minutes. To record evoked action potentials a series of 20 200ms current steps were applied and the resulting current response recorded. If no events were visible in the first attempt the step size was increased from 2pA to 10pA. Both spontaneous and evoked action potentials were detected and quantified using a MATLAB script.

Calcium imaging

50 µg Rhod-4™ (AAT Bioquest) were dissolved in 49.21 µl DMSO to generate a 1mM stock and aliquots were kept at -20°C.

Neurons were incubated with 4 µM Rhod-4 (3 µl stock solution in 750 µl Neurobasal complete media, see Supplementary Information Methods 1) for 30 min at 37°C, 5% CO2, 100%

humidity. Cells were washed three times with prewarmed media. And left to recover for 45 min at 37°C, 5% CO2, 100% humidity.

Each dish was imaged at 37°C for less than 30 min with a Leica DMi8 using a ×63 oil objective (numerical aperture 1.4) and a YFP filter set. Approximately 10 fields of view were imaged per dish while avoiding cell clusters. For each FOV, we recorded one picture every 80ms for approximately 40 seconds. Files were saved in .lif format.

Tetrodotoxin treatment

Tetrodotoxin (TTX) treatment was performed to test calcium peaks for dependence on voltage-gated sodium channels at DIV 7. For TTX treatment, cells were exposed to 0.1µM TTX for 2 minutes prior to imaging. In contrast to the control cells, none of the TTX-treated cells showed any activity (see Extended Data Fig. 8). This suggests that the calcium peaks we detected were triggered by action potentials.

Analysis of calcium imaging data

.lif files were converted into .tiff & .png files with a custom Python script utilising the readlif library. Cell labelling initially used supervise.ly and later Label Studio. A neural net based on the U2-Net[43] was trained on manually labelled images and used for automated segmentation. The automated segmentation results were manually validated and adjusted (Fig. 2a).

Cell activity was quantified using our custom Python software which is available at https://gitlab.com/rknt/cell-activity-from-calcium-imaging. Cell segmentation data was read as well as the .tiff files from each FOV the average fluorescence intensity was determined within each cell outline as a function of time (Fig. 2b). For each intensity profile, a polynomial baseline was fitted (using peakutils.baseline) which correlates with the bleaching of the fluorescent dye inside the respective cell. The fluorescent intensity was normalized using with the baseline and smoothed using a Butterworth filter (using scipy.signal.butter) (Fig. 2b). Then a peak finder

(scipy.signal.find_peaks) was applied to the filtered data and the peak prominence, the peak width and peak length of each peak were determined. In addition, the variance of each normalised trace was determined.

Cells were classified as "active" if they had at least one peak that exceeded certain threshold criteria (Fig 2c) and variance in their normalised signal that exceeded a threshold variance (see Extended Data Fig. 6). The thresholds were optimised using a training set of 77 calcium imaging series that had been manually analysed (see Extended Data Fig. 7). Using the following values automated analysis reached a sensitive of 94% and a specificity of 99% when compared to the manual analysis: peak prominence = 0.023, peak width = 0.1, maximum peak length = 37, and variance = 10^{-4}. These values were used for all subsequent quantification of cell activity. The active fractions of FOVs across conditions were compared using a Kruskal-Wallis test and Tukey post-hoc test.

In order to assess the efficacy of the automated analysis procedure, a manual analysis was conducted on 92 FOVs comprising 1281 cells. This involved viewing the videos and noting in a spreadsheet whether or not each cell exhibited observable activity. The manual and automatic results were then compared in terms of the number of active cells in each FOV. During this process, it became evident that our manual approach was prone to errors. Upon conducting a comparison between manual and automated analyses, we discovered numerous active cells that had escaped manual detection. Upon reviewing the videos, we realised that the discrepancies largely stemmed from instances where we had visually overlooked certain activities. Consequently, we corrected the spreadsheet where necessary and repeated the process. Extended Data Figure 7 shows the difference between the numbers of active cells that we determined to be active by visual inspection and automated analysis. In 76 out of 92 FOV, the two methods agreed on the activity every single cell. Analysing the sensitivity *sn* and specificity *sp* of the signal detection (assuming the manual analysis as ground truth), we found sn=96%, and sp=98%.

Western Blots

Experimental procedure WBs

All buffers and media used in this protocol are listed in the Supplementary Information Methods 1. WT hippocampal neurons were grown on hydrogels as described above. At DIV 7, one dish at a time was processed: cells were washed once with PBS (at RT), covered with 300 µl ice cold Magic RIPA Buffer media containing 1% protease and phosphatase inhibitor cocktail and left on ice on a shaker for 20 minutes. After 20 minutes, the next dish of identical background was washed with PBS and the lysate butter from the first dish was carefully pipetted to the second dish which then was left on the shaker on ice for 20 mins. This procedure was repeated with all 15 dishes of the same condition. In the end, the lysate buffer was transferred into a 1.5 ml Eppendorf tube and kept at -80°C for further processing.

The protein concentration was measured using a Bradford Assay. The samples were diluted to 1mg/ml and 0.5mg/ml protein concentration in LDS sample buffer (Nupage NP007) with 5% (v/v) beta-mercaptoethanol, respectively (see below). The samples were denatured on a heat block at 95°C for 5 minutes before loading them on to the PAGE gels.

Depending on the size of the protein, either a 4-20% or 4-12% gradient gels were used for the blots. Each lane was loaded with 20µL sample or with the protein ladder. Gels were run at RT at 40mA using MOPS SDS running buffer.

The gels were washed in transfer buffer and blotted using the Biorad Mini PROTEAN Transfer System in a cold room (4°C) for 16h at 21V.

For probing, the membranes were dried for 1 hour at RT and all following procedures were performed on a shaker at RT. After wetting with TBS for 5 mins, the membranes were blocked in 5% milk in TBS for 30 mins and probed with the appropriate antibody dilution in 5% milk in TBST

for 1 hour. After 3 washes with TBST the membranes were probed with the appropriate HRP conjugated secondary Antibody for 1 hour in 5% milk in TBST, and washed in TBST before the ECL reactions were carried out. Imaging was performed using the LiCor Odyssey FC. For Total Protein Stains (TPS) the Li-Cor Revert 700 reaction was performed according to user instructions and the membranes imaged using the 700 nm channel of the LiCor Odyssey FC.

Antibodies used in these WBs at the following concentrations:

- Piezo1, rabbit, polyclonal (Novus Biologicals, NBP1-78446, 1:1000)
- TTR, rabbit, polyclonal (Invitrogen, PA5-27220, 1:500)
- Glur1 = GRIA1, mouse (antibodiesinc, N355/1, 1:500), and mouse (BioLegend, #819803, 1:500), and rabbit (Alomone Labs, AGC-004, 1:500)
- GABAR, rabbit (Sigma, A90903, 1:1000)
- NMDAR, rabbit (GeneTex, GTX109713, 1:1000)
- Alpha Tubulin, mouse (abcam, ab7291, 1:20000)
- GAPDH, mouse (Proteintech, PT6004, 1:20000)
- Goat anti-mouse (acbcam, ab6789, 1:10000)
- Goat anti-rabbit (abcam, ab97080, 1:10000)

WB analysis

General analysis of WB normalisation proteins were selected individually for each protein stain by conducting Western blots (WBs) of a titration series of the same protein lysates and identifying those that provided the most consistent signals across dilutions. For Piezo1 and TTR, total protein staining was used for normalisation, whereas NMDAR, GLUR1, and GABAR were normalised using tubulin.

The protein bands were analysed using Image Studio Lite by Licor. The resulting data were saved in .csv files and normalised and plotted with a custom-written Python script. To test the

signal quality in our Western blots, we compared the signals of the lanes loaded with lysates of 1 mg/ml protein concentration (normal concentration) and those loaded with lysates of 0.5 mg/ml protein concentration (low concentration). If the signals were in the linear range, the normalised signals of the normal protein concentration lanes would be expected to be similar to those of the low concentration lysates.

Analysis of WBs for pathway analysis

First, WB bands were analysed as described above. Then, the ratio of the WB signals between lysates of cells grown on soft gels and lysates from cells grown on stiff gels was calculated. Subsequently, the ratio **r** was evaluated.

$$r = \frac{normalised\ signal_{soft}}{normalised\ signal_{stiff}}$$

Multiple biological replicates were processed (n>3), each with multiple blots and technical replicates. To calculate **r**, the median of the normalised signal for each band was determined for each biological replicate, blot, technical replicate, and lysate concentration. The ratio was then built between the median from the lysate of cells grown on soft gels and the lysates from cells grown on stiff gels.

If **r < 1** for the lysate of one protein concentration but **r > 1** for the lysate of the other protein concentration on the same blot, the blot was discarded.

Specific analysis of the Transthyretin bands

Transthyretin (TTR) was blotted on two different gels: 4-20% gels and 4-12% gels.

In its functional form, TTR is a tetramer (dimer of dimers). The fraction of this tetramers which was broken down to its monomeric form during the linearisation process in the WB protocol, is unclear. We expected to see 3 bands associated with the monomer, the dimer and the tetramer. In order to blot all these bands, we found that we had to combine two different gel

substrates, 4-20% gels for the low molecular weight bands (usually only mono and dimer) and 4-12% gels for the higher molecular weight bands (usually only dimer and tetramer).

Since the strength of the signals corresponding to the monomer and dimer were very weak compared to the tetramer and could often not be quantified, we concluded that most tetramers were not degraded. Therefore, only tetramer bands were considered in the pathway analysis experiments.

RNA purification

RNA was purified using the Qiagen RNeasy plus Micro Kit (#74034).

Hippocampal neurons were cultured (as described above) on hydrogels of different stiffnesses for 7 days. The culture medium was removed and 350 µl RLT plus buffer (Qiagen Kit #74034) containing beta-mercaptoethanol was added. The gels were scraped from the dish and transferred to a 1.5 ml Eppendorf tube. Each sample was vortexed for 30 seconds and then homogenised by pipetting up and down (x50) using a cut pipette tip. Afterwards, the RNA purification protocol was carried out as described in the manual and total RNA was diluted with 20 µl of RNase-free water. The 70% and 80% ethanol, as well as RLT plus beta-mercapto buffer were freshly prepared. The RNA concentration was determined using a nanodrop. The measured concentrations varied between 10 and 100 ng/µl.

RNA sequencing and analysis

The RNA samples were sequenced by Cambridge Genomic Services (CGS) using their low input RNA assay. Raw fastq files were submitted to EMBL-EBI ArrayExpress with accession number E-MTAB-13503 (https://www.ebi.ac.uk/biostudies/arrayexpress/studies/E-MTAB-13503). Single end, 75 bp length RNA sequence quality control was performed using fastqc (version 0.11.9)[44], TrimGalore (version 0.6.6)[45], then aligned to the Rattus Norvegicus genome (Rnor_6.0) using STAR (version 2.6.1d)[46], and gene counts were generated using HTSeq (subread version 2.0.1)[47]. The

above analysis was performed by CGS. The summary of the mapping statistics and number of genes identified for each library is given in the respective table (Supplementary Information Data 1).

Differential expression (DE) analysis was mainly performed using the R software (version 4.2.3) DEseq2 (version 1.38.3)[48] pipeline. All possible pairwise comparisons were performed. Normalized counts for fully differentially expressed genes (DEGs) and the lists of paired DEGs can be found in supplementary tables 2-11 under https://github.com/xz289/Kreysing_Franze. DESeq2 generated an individual gene counts plot, which was normalised using the median of ratios method. The counts were divided by sample-specific size factors determined by the median ratio of gene counts relative to the geometric mean per gene. The normalised counts were then log2 transformed. Furthermore, for each comparison, a principal component analysis (PCA) plot and a volcano plot were generated.

Immunocytochemistry of CRISPR KD and TTR KD neurons

To fix samples, half the media was removed and replaced with 4% PFA and 15% sucrose for 30 minutes. Samples were washed 9 times with PBS. Samples were permeabilized for 5 min in 0.1% Triton X. They were washed 3 times with 0.0001% Triton X in PBS and subsequently blocked with 5% serum, 0.0001% Triton in PBS (blocking solution) for 45 min at room temperature. Afterwards, the samples were incubated with the primary antibody overnight at 4°C in blocking solution and washed 5 times with 0.0001% Triton in PBS. This was followed by incubation with the secondary antibody for 45 min at room temperature in blocking solution. The samples were washed 5 times in PBS with 0.0001% Triton X. If stained for the nucleus, the samples were then incubated with DAPI (Merck, D5942, working concentration: 0.1 µl/ml) in PBS with 0.0001% Triton X for 20 min. Finally, the samples were washed 5 times in PBS and mounted with 9 µl Fluromount-G Mounting Medium (Thermo Fisher Scientific #00-4958-02) and a 18mm coverslip. The primary

antibodies used were TTR (Thermo Fisher, PA5-20742, chicken, 1:400), Piezo1 (proteintech, 28511-1-AP, rabbit, 1:50), and β-tubulin (synaptic systems, #302304, guinea pig, 1:500). The secondary antibodies were goat anti-chicken Alexa Fluor Plus 405(Thermo Fisher, A48260, 1:500), donkey anti-guinea pig 647 (Jackson Immuno Research, 706-605-148, 1:500), and donkey anti-rabbit Alexa Fluor 488 (Thermo Fisher, A-21206, 1:500) Images were taken using a Leica TCS SP8 confocal microscope with a 63x oil objective (NA=1.4).

Quantitative analysis of the immunostainings was performed using the total intensity values of each channel. The Piezo1 signal was most abundant in the somata. For the Piezo1 KD cells and the control cells, Piezo1 signals were normalised by dividing with the DAPI signal (Extended Data Fig. 3). For TTR KD cells and the control, TTR and tubulin were quantified (Extended Data Fig. 10). TTR was normalised by dividing with the tubulin signal because TTR was strongly expressed along the neurites.

TOPO TA cloning and DNA sequencing of CRISPR edited neurons

Genomic DNA from CRISPR-edited primary hippocampal cultures and CTRL cultures was prepared using the Qiagen DNeasy Blood and Tissue Kit (Cat # 69504). For analysis of CRISPR target sites, PCR primers were designed to amplify the targets of one guide each for Piezo1 KD1 (guide #7, see Methods on Piezo 1 guides) and KD2 (guide #8, see Methods on Piezo 1 guides) and the targets of TTR KD guides #1 and #2 (see Methods on TTR guides) using the All Taq Master Mix Kit Qiagen (Cat # 203144). PCR reactions were performed on a Biorad T100 thermal cycler as follows 2 min 95°C denaturation; 40 cycles: 5 sec 95°C, 15 sec 55°C, 10 sec 72°C; and final extension 5 min 72°C. PCR amplicons were gel purified using the NEB Monarch DNA Gel Extraction Kit (Cat # T1020S) and cloned into either the PCRII Dual Promoter TOPO vector using the Invitrogen TOPO TA Cloning Kit (Cat # 45-0640) or the PCR 2.1 TOPO vector using the TOPO TA Cloning Kit (Cat # 45-

0641). Sanger sequencing was performed using the M13F primer. Sequence analysis was performed in a custom written Python script using the Bio package.

Xenopus laevis rearing

All experiments involving *Xenopus laevis* were conducted in compliance with the Ethical Review Committee of the University of Cambridge and the UK Home Office. *Xenopus laevis* embryos were obtained through *in vitro* fertilisation and reared in 0.1 x Marc's Modified Ringers solution (MMR, see Supplementary Information Methods 1) at 14-18°C until they reached the desired developmental stages for the experiments. The embryos were staged according to[49]. All embryos used in this study were below embryonic stage 45.

Xenopus laevis brain exposure and transglutaminase treatment

Xenopus laevis embryos were prepared for TG treatment and atomic force microscopy (AFM) measurements as described previously[14]. At stage 33, *Xenopus laevis* embryos were anaesthetised using exposed brain medium (EBM, see Supplementary Information Methods 1). The embryos were immobilised in a silicone filled (SYLGARD™ 184 Silicone Elastomer, cured) Petri dish using bent 0.2 mm minutien pins (Austerlitz). The skin and eye primordium were removed from one side, and one of the brain hemispheres was exposed from the dorsal to ventral midline, and from the hindbrain to the telencephalon using 0.1/0.15 mm minutien pins (Austerlitz) in pinholders. The embryos that were exposed were used for subsequent experiments. To increase the stiffness of brain tissue, 0.5 mg/ml (corresponds to 1 unit per 581 µl) TG (Sigma, T5398) was added to the EBM. Control embryos were kept in EBM. Both conditions were kept at 20-21°C overnight until they reached stage 37.

Xenopus laevis brain AFM measurements

For AFM stiffness mapping, embryos were prepared as described above. The immobilised embryos which had their brains exposed were then incubated in TG or left in a control solution for

at least two hours prior to measurement. The spring constant (k) of tipless silicon cantilevers (Arrow-TL1, Nanoworld) was determined using the thermal noise method. Cantilevers with k values between 0.02-0.04 N/m were selected for the experiments. Polystyrene beads with a radius of 37 μm (microParticles GmbH) were glued to the cantilevers. Subsequently, the cantilevers were mounted on a CellHesion-200AFM head (JPK instruments). Force measurements and data analysis based on the Hertz model were done using custom scripts previously described[14,15].

Xenopus laevis brain FM1-43 imaging and analysis

First, dishes for mounting the embryos for imaging were prepared. For each sample, two adhesive stationary hole reinforcement rings were glued as a stack in the centre of a 35 mm ibidi dish (ibidi #81218-200). FM1-43 (Thermo Fisher Scientific T3163) stock solution was prepared at 1 mg/ml in distilled water. For live staining of embryonic brains, the solution was dissolved at a ratio of 1:200 in EBM. The embryos were incubated at room temperature for 5 min, washed 3 times, and then placed brain-side down in the centre of the adhesive rings in the pre-prepared dishes. A coverslip was then placed on top of the rings to prevent any movement of the sample.

The embryos were imaged using a spinning disk confocal microscope (Leica SP8) with a DS RED filter set and a 10x objective (NA=0.32). The images were analysed using FIJI. The confocal stack was limited to the in-focus slides and averaged. In order to quantify these signals, we measured the fluorescent intensity in a 100-pixel-wide stripe across the area corresponding to the supraoptic tract (Fig. 4c). The maximum and mean intensity were determined for each line profile and the ratio maximum/mean intensity was calculated. This ratio was compared between the different conditions using a Mann-Whitney test.

Immunohistochemistry of _Xenopus laevis_ brains

For whole brain immunostaining, embryos were prepared as described above. The exposed embryos were then incubated in TG or left in a control solution overnight. At stage 37, embryos

were fixed in 4% PFA in PBS for 1 hour, followed by two washes in PBS. The brains were then dissected out of the embryos in PBS with 0.1% Triton X, using 0.1/0.15 mm minutien pins (Austerlitz) in pinholders. The brains were washed for 30 min in PBT (PBS with 0.2% BSA and 0.1% Triton X). This was followed by blocking in PBT with 10% donkey serum for 45 min. Brains were incubated with a primary mouse anti-acetylated-tubulin antibody (Sigma, T6793, 1:300 in PBT) at 4°C overnight. The brains were then washed 3 times in PBT. Brains were then incubated with a secondary donkey anti-mouse antibody (Invitrogen, A10037, 1:300) in PBT with 10% donkey serum for 2 hours at room temperature. The brains were then washed three times in PBS and incubated with phalloidin 488 (1:200) and DAPI (1:10000) in PBS. Finally, they were washed 5 times with PBS and mounted in ibidi dishes as described in the FM1-43 imaging section. The embryos were imaged using a confocal microscope (Leica SP8) and a 40x oil immersion objective (NA=1.3). The images were processed using FIJI, creating a maximum intensity projection of all slices containing the axonal tract signals. The acetylated tubulin staining reveals the location of axon tracts.

Acknowledgements

We would like to thank Prof. Dr. Christine Holt for discussions and advice, and Liz Williams, Rachel McKeown, and Julia Becker for preparing hydrogels and mental support as well as Sebastián Vasquez Sepulveda for sharing FIJI expertise. We acknowledge funding by the Wellcome Trust (PhD studentship 222280/Z/20/Z to S.M.), Cambridge Trust (scholarship to S.M.), ESPRC (research grants EP/R025398/1 and EP/Y008715/1 to L.M.), BBSRC (research grant BB/N006402/1 to R.T.K. and K.F.), the European Research Council (Consolidator Award 772426 to K.F.), the German Research Foundation (DFG) (projects 460333672 CRC1540 EBM and 270949263 GRK2162 to K.F.) and the Alexander von Humboldt Foundation (Alexander von Humboldt Professorship to K.F.).

Contributions

E.K., H.G., R.T.K., K.F. designed the study. H.G.: performed the immunostaining of synapses and patch clamp experiments. E.K. developed the CRISPR-Cas9 protocols and performed the calcium imaging experiments. E.K. & K.M. performed the RNA sequencing experiments and WB experiments. E.K. analysed the WBs. E.K. & S.M. carried out the *Xenopus laevis* TG stiffening and imaging. A.W. performed the AFM measurements. L.M. wrote the code to analyse the synapse density immunostaining. E.K. & D.H. wrote the calcium imaging analysis pipeline, the immunostaining quantification code for KD cells, the *Xenopus laevis* synapse analysis code, the WB quantification code. K.M. performed the TOPO cloning. E.K. wrote the code to analyse the DNA sequences. X.Z. performed the RNA-sequencing analysis. E.K. performed the pattern analysis of the RNA sequencing results. R.H. & R.T.K. performed the patch clamp data analysis. A.D. supported neuronal cell culture during lockdown. E.K.P. prepared hydrogels for synapse immuno staining

experiments. E.K. and K.F. wrote the manuscript, with contributions from all co-authors. K.F. supervised the project.

Competing Interests

The authors declare no competing interests.

Additional Information

Correspondence and requests for materials should be addressed to: Eva Kreysing (emk42@cam.ac.uk), Ragnhildur Thóra Káradóttir (rk385@cam.ac.uk), Kristian Franze (kf284@cam.ac.uk)

Supplementary Information is available for this paper.

Data Availability

The datasets generated and/or analysed for this study are available as follows.

Raw RNA data: https://www.ebi.ac.uk/biostudies/studies/E-MTAB-13503.

Processed RNA data: DOI: 10.5281/zenodo.12742961

Remaining data: DOI: 10.5281/zenodo.12802682

Code Availability

Code used for the analysis of cell activity from calcium imaging is available in the Gitlab repository https://gitlab.com/rknt/cell-activity-from-calcium-imaging. The code for analysing

synaptic densities of immunostainings can be found in the repository https://github.com/lemur01/synpasestat.

Extended Data

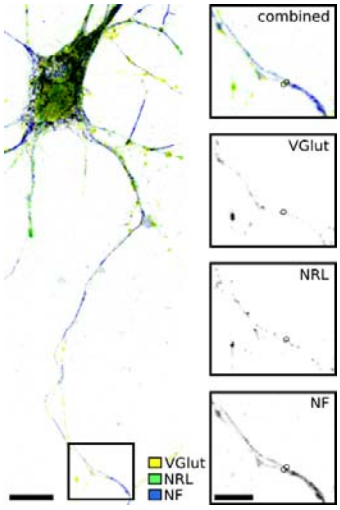

Extended Data Figure 1 | Detection of synapses The main panel shows a complete field of view (FOV) of neurons grown on a stiff substrate. The insets show the same area in the three channels relevant for this synapse: the presynaptic vesicular glutamate transporter (VGlut), postsynaptic neuroligin (NRL), and neurofilament (NF). Synaptic markers were identified to be co-localised if their intensity maxima (indicated by circles) were located within two pixels distance and colocalize with the NF signal. Scale bar in the main panel is 10 µm, in the insets 5µm.

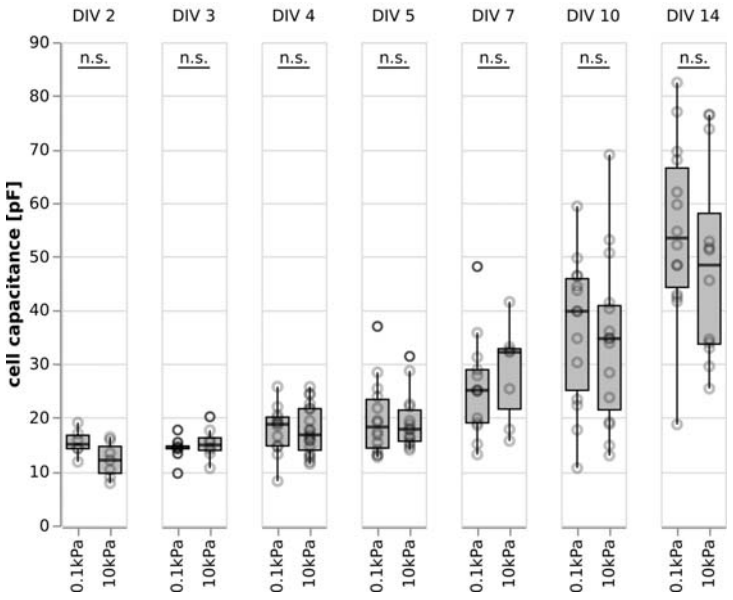

Extended Data Figure 2 | Cell capacitance as a function of time in culture and substrate stiffness. The capacitance of neurons was plotted at DIV 2-DIV 14. The capacitance increases over time on both substrates. It does not depend on substrate stiffness (two-tailed t-tests).

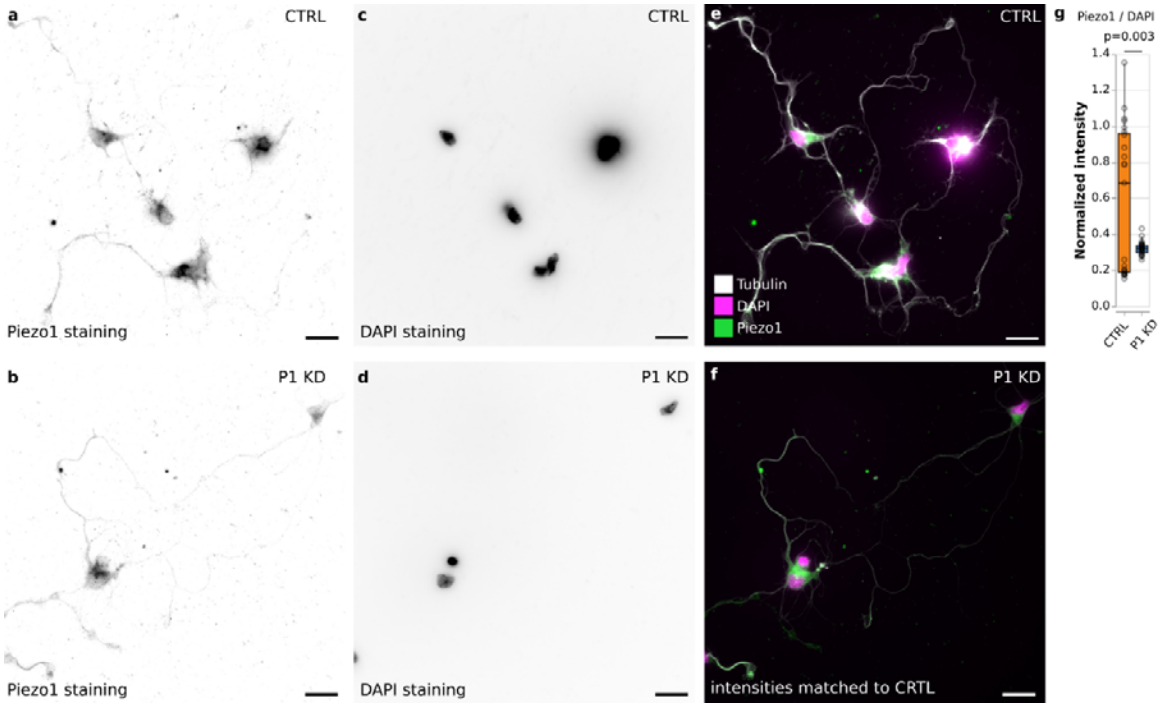

Extended Data Figure 3 | Characterization of Piezo1 KD in primary neurons. Stainings for individual proteins were intensity-matched between the two conditions. (a, c, e) CTRL neurons and (b, d, f) P1 KD neurons were stained for (a, b) Piezo1 and (c, d) nuclei (DAPI). (e, f) Piezo1, DAPI, and tubulin signals overlaid. (g) The intensities for each field of view (FOV) for the Piezo1 and the DAPI channels were calculated and normalised (see methods). Piezo1 expression was significantly reduced in the KD condition (two-tailed t-tests). For either condition, 23 FOVs were quantified. Scale bars: 20 µm.

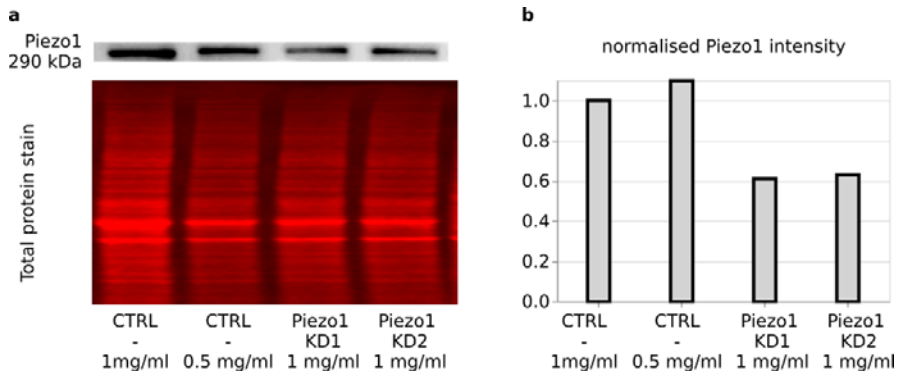

Extended Data Figure 4 | Western blots of CTRL and Piezo1 KD neurons. (a) Representative Western blots (WB) for the CTRL, Piezo1 KD1, and Piezo1 KD2 neurons. The protein lysates have been blotted at a protein concentration of 1mg/ml. For the CTRL cells, an additional lane has been run at 0.5 mg/ml protein concentration to check for linear behaviour of the WB quantification. The top row shows the Piezo1 stain, the bottom the total protein stain (TPS) used for normalisation. (b) Quantification of WBs. The normalised signals for CTRL cells are similar between 1 mg/ml and 0.5 mg/ml protein concentration, confirming the linearity of the signal. The CRISPR Cas9 Piezo1 KD conditions showed a signal reduction by about 40%.

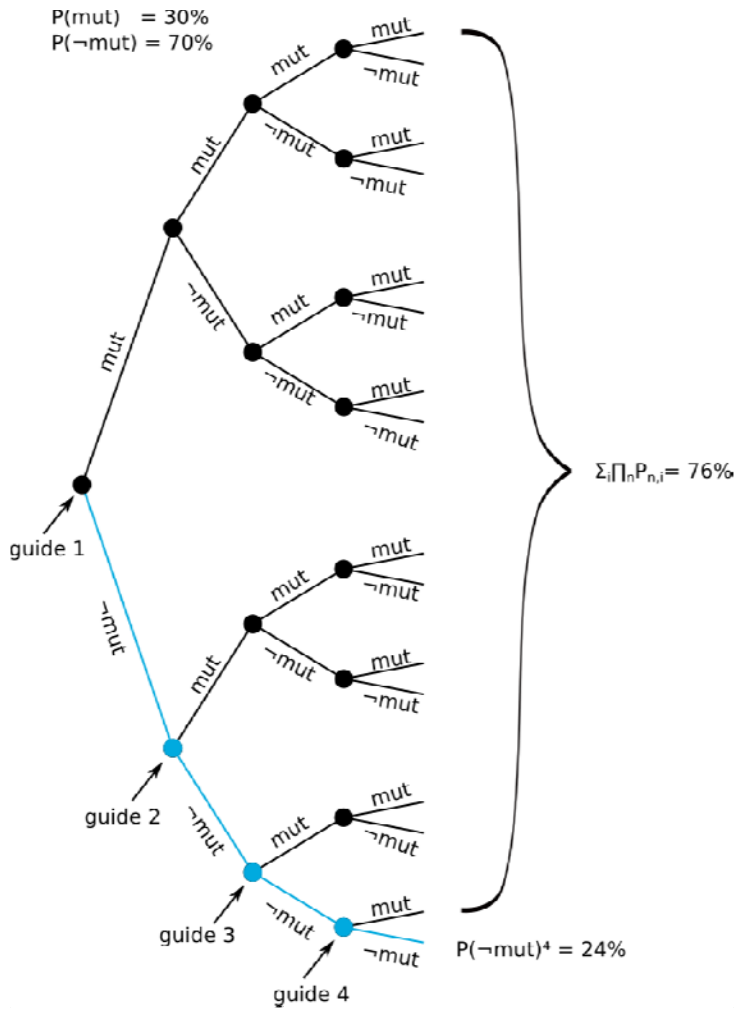

Extended Data Figure 5 | Probability tree for *Piezo1* guides introducing mutations in the *Piezo1*-gene. The probability for alterations in the *Piezo1* gene if 4 CRISPR/Cas9 guides are used simultaneously was calculated. It was assumed that each CRISPR guide has a 30% chance of successfully editing a gene and that the guides do not interfere with each other. For each individual gene, there is a 70% chance that a single guide will fail to edit the gene. So the probability that none of the four guides will edit the gene is 0.7^4 = 0.24 = 24%. This means that there is a 24% chance that the gene will remain completely unaltered by any of the guides. Vice versa, 76% of the time at least one of the guides will successfully edit the gene, resulting in mutations at one or more sites.

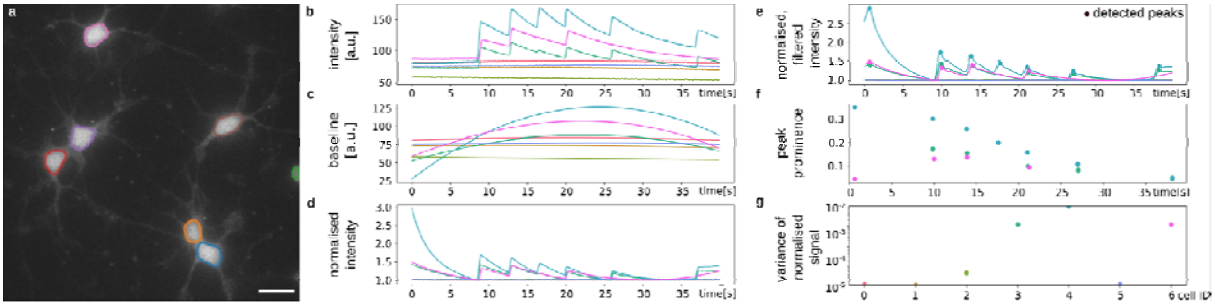

Extended Data Figure 6 | Step-by-step description of the peak detection algorithm. (a) FOV in calcium imaging series with outlined somata. (b) Raw intensity traces for each cell. (c) 3rd degree polynomial fit of the baseline for each trace. (d) The signals were normalised by dividing the raw signal by the baseline. (e) Signals after processing with Butterworth filter and detected peaks. (f) Peak prominence of each detected peak. (g) Peak height of each detected peak. Scale bar is 25 µm.

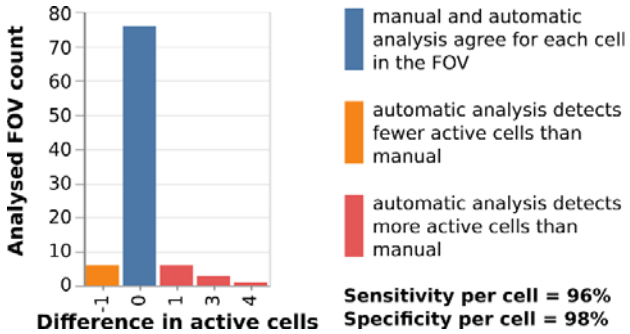

Extended Data Figure 7 | Quality check of the automated calcium analysis pipeline. 1281 cells from 92 FOVs were analysed manually and by the algorithm described in the Methods. We found a very good agreement between the two analysis approaches, indicating a high sensitivity and specificity of the automated detection of calcium peaks.

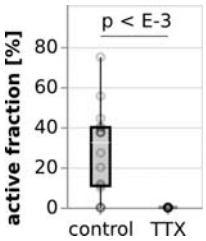

Extended Data Figure 8 | Perturbation of action potentials. The application of the neurotoxin Tetrodotoxin (TTX), which binds to voltage-gated sodium channels in neurons and thus inhibits action potentials, depleted the calcium transients observed in CTRL neurons cultured at DIV 7 (Mann-Whitney U test), indicating that the observed calcium transients were caused by the electrical activity of neurons.

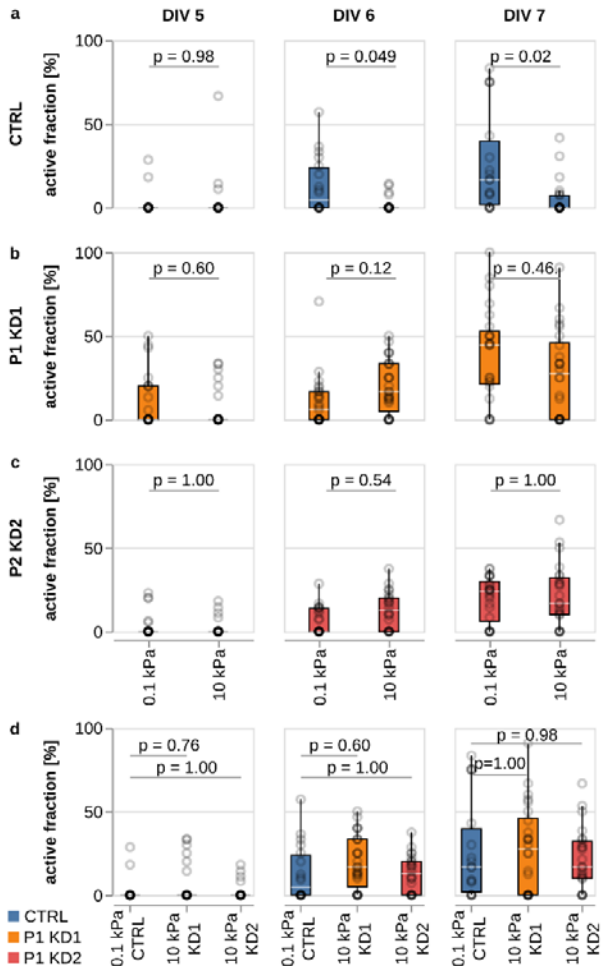

Extended Data Figure 9 | Extended comparison of neuronal activity as a function of substrate stiffness, time in culture, and Piezo1 expression. (a) From DIV 6, the activity of CTRL neurons is significantly higher on soft than on stiff substrates (Kruskal-Wallis test followed by Tukey posthoc test). (b, c) In Piezo1 KD neurons, the activity of the cells is independent of substrate stiffness. (d) The activity of CTRL neurons on soft substrates is similar to the activity of Piezo1 KD cells on stiff substrates, indicating that stiff substrates activate Piezo1, which then slows down electrical maturation of neurons. Data replotted from Fig. 2g.

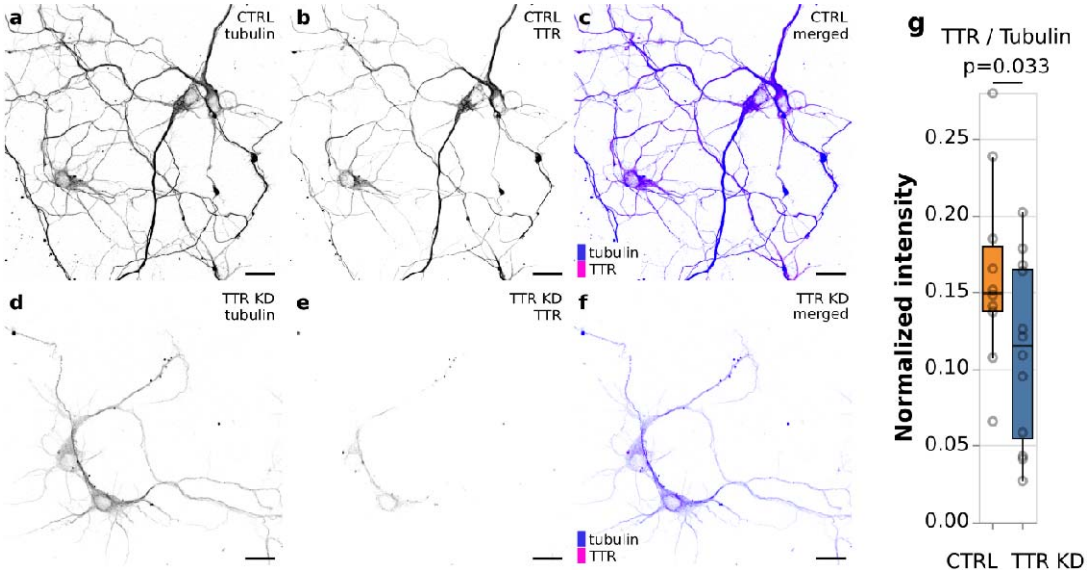

Extended Data Figure 10 | TTR KD in primary neurons. Stainings for individual proteins were intensity-matched between the CTRL neurons (a-c) and TTR KD neurons (d-f). (a) Tubulin staining and (b) TTR staining of CTRL cells (merged in (c)). (d) Tubulin staining and (e) TTR staining of TTR KD cells (merged in (f)). (g) Quantification of fluorescence signals. The total TTR signal per FOV was normalised to the total tubulin signal. We found a significant reduction of TTR in the KD condition (one-tailed t-test). n_{CTRL} = 10 FOV, n_{TTRKD} = 12 FOV. Scale bars: 20 µm.

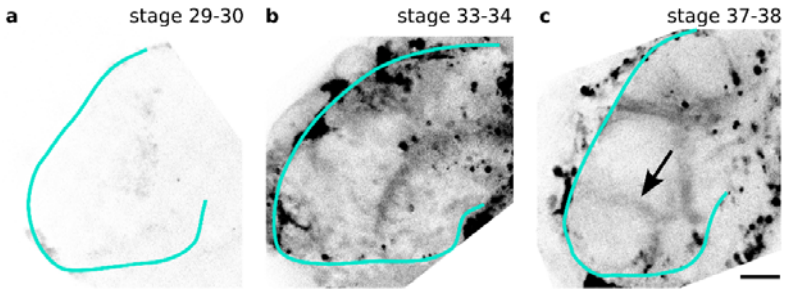

Extended Data Figure 11 | Synapse patterns in developing *Xenopus laevis* brains. (a-c) Exposed *Xenopus laevis* brains labelled with the synaptic marker FM1-43. (a) At stage 29-30, no synapses are visible yet. (b) At stage 33-34, some first synaptic patterns emerge in the diencephalon. (c) From stage 37-38 onwards, brains of wild type animals showed a characteristic pattern of synapses, including a semicircle surrounding the telencephalon coinciding with the position of the supraoptic tract (arrow). All images are intensity matched. Outlines of brains indicated by green line. Scale bar: 100 µm.

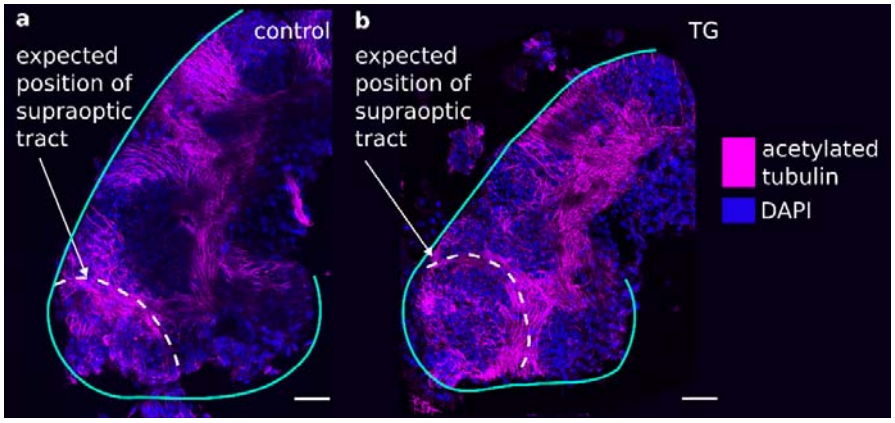

Extended Data Figure 12 | Axon tract formation is unaffected by TG treatment. Acetylated tubulin staining revealed the location of axon tracts. The characteristic patterns form in both (a) control and (b) TG-treated brains. White dashed curves indicate the areas of the supraoptic tract. Outlines of brains indicated by green curves. Scale bars: 50 µm.